EFFECTS OF PULSE PARAMETERS ON SURFACE PROPERTIES OF SILVER
COATINGS ON COPPER SUBSTRATES

A THESIS SUBMITTED TO
THE GRADUATE SCHOOL OF NATURAL AND APPLIED SCIENCES
OF
MIDDLE EAST TECHNICAL UNIVERSITY

BY

CANER BAŞARAN

IN PARTIAL FULFILLMENT OF THE REQUIREMENTS
FOR
THE DEGREE OF MASTER OF SCIENCE
IN
METALLURGICAL AND MATERIALS ENGINEERING

SEPTEMBER 2019

Approval of the thesis:

**EFFECTS OF PULSE PARAMETERS ON SURFACE PROPERTIES OF SILVER COATINGS ON COPPER SUBSTRATES**

submitted by **CANER BAŞARAN** in partial fulfillment of the requirements for the degree of **Master of Science in Metallurgical and Materials Engineering Department, Middle East Technical University** by,

Prof. Dr. Halil Kalıpçılar
Dean, Graduate School of **Natural and Applied Sciences**       _____

Prof. Dr. Cemil Hakan Gür
Head of Department, **Met. and Mat. Eng.**       _____

Prof. Dr. İshak Karakaya
Supervisor, **Met. and Mat. Eng., METU**       _____

**Examining Committee Members:**

Prof. Dr. Kadri Aydınol
Met. and Mat. Eng., METU       _____

Prof. Dr. İshak Karakaya
Met. and Mat. Eng., METU       _____

Assist. Prof. Dr. Metehan Erdoğan
Met. and Mat. Eng., AYBU       _____

Assist. Prof. Dr. Erkan Konca
Met. and Mat. Eng., Atılım University       _____

Assist. Prof. Dr. Batur Ercan
Met. and Mat. Eng., METU       _____

Date: 05.09.2019

**I hereby declare that all information in this document has been obtained and presented in accordance with academic rules and ethical conduct. I also declare that, as required by these rules and conduct, I have fully cited and referenced all material and results that are not original to this work.**

Name, Surname: Caner Başaran

Signature:

**ABSTRACT**


**EFFECTS OF PULSE PARAMETERS ON SURFACE PROPERTIES OF SILVER COATINGS ON COPPER SUBSTRATES**

Başaran, Caner
Master of Science, Metallurgical and Materials Engineering
Supervisor: Prof. Dr. İshak Karakaya

September 2019, 100 pages

Electronic conductivity is a parameter that exhibits the free-electron transportation ability of a material. The radiation efficiency and insertion loss are directly related to the conductivity of the materials used in the systems like antennas, waveguides, power dividers, couplers, active circuit elements etc. operating at Millimeter-Wave (mmW) and Terahertz (THz) frequencies. The signal quality of systems operating at ultrahigh frequencies for the transmission of electromagnetic waves is very much dependent on the surface finish that has good conductivity. The use of pulse electrodeposition techniques causes homogenous deposits of better surface quality than direct current techniques. The effects of pulse parameters on the surface quality of silver coatings on the copper base material in terms of scattering parameter (S-parameter) and surface roughness were analyzed in this study. Three pulse parameters which are duty cycle, frequency and average current density were selected to observe the effects on the surface quality of silver plating. It was analyzed that the increasing average current density has the effect of reducing surface roughness. Moreover, the surface roughness was reduced while increasing on time of the pulse current. Increasing the time differences between on time and off time also caused smoother surfaces. Relatively rough surfaces were observed at higher duty cycle and lower frequency. Furthermore,

it was detected that frequency was less effective on surface roughness. As a result of (S11) measurements, it was observed that rougher surfaces have more return loss.

Scanning Electron Microscope (SEM) was used to characterize the microstructure of silver plating. As a result of SEM analysis, pyramidal growth was obtained with pulse electrodeposition. Smaller grains and less porosities were detected with the increasing average current density at high frequencies and high duty cycles. Irregularity was observed in the grain structure with decreasing average current density. According to X-Ray diffraction (XRD) analysis, smaller silver grains were observed at high duty cycle, high frequency and high average current density. Effects of pulse parameters on the diffusion of silver into the copper base material were analyzed by Energy-dispersive spectrometer (EDS) line analysis.

# ÖZ

## BAKIR ÜZERİNE KAPLANAN GÜMÜŞÜN YÜZEY ÖZELLİKLERİNE DARBE PARAMETRELERİNİN ETKİSİ

Başaran, Caner
Yüksek Lisans, Metalurji ve Malzeme Mühendisliği
Tez Danışmanı: Prof. Dr. İshak Karakaya

Eylül 2019, 100 sayfa

Elektronik iletkenlik, bir malzemenin serbest elektron taşıma kabiliyetini gösteren bir parametredir. Radyasyon verimi ve geçiş kaybı, milimetre-dalga (mmW) ve Terahertz (THz) frekanslarında çalışan antenler, dalga kılavuzları, güç bölücüler, bağlaştırıcılar, aktif devre elemanları vb. sistemlerde kullanılan malzemelerin iletkenliği ile doğrudan ilgilidir. Elektromanyetik dalgaların iletimi için çok yüksek frekanslarda çalışan sistemlerin sinyal kalitesi, iyi iletkenliği olan yüzey kaplamasına çok bağlıdır. Darbeli elektro çöktürme tekniklerinin kullanılması, doğru akım tekniklerinden daha iyi yüzey kalitesinde homojen birikintilere neden olur. Bu çalışmada, darbe parametrelerinin, bakır taban malzemesi üzerindeki gümüş kaplamaların yüzey kalitesine etkileri, saçılma parametresi (S-parametresi) ve yüzey pürüzlülüğü açısından incelenmiştir. Gümüş kaplamanın yüzey kalitesi üzerindeki etkilerini gözlemlemek için üç darbe parametresi görev döngüsü, frekans ve ortalama akım yoğunluğu seçilmiştir. Ortalama akım yoğunluğunun artmasının yüzey pürüzlülüğünü azalttığı analiz edilmiştir. Ayrıca, darbe akımının açık kaldığı süre arttırılırken yüzey pürüzlülüğü azaltılmıştır. Akımın açık ve kapalı zamanları arasındaki farkın artması, daha pürüzsüz yüzeylere neden olmuştur. Daha az pürüzlü yüzeyler daha yüksek görev döngülerinde ve daha düşük frekanslarda gözlemlenmiştir. Ayrıca, frekansın yüzey pürüzlülüğü üzerinde

daha az etkili olduğu tespit edilmiştir. (S11) ölçümleri sonucunda pürüzlü yüzeylerin daha fazla geri dönüş kaybına neden olduğu gözlemlenmiştir.

Gümüş kaplamanın mikro yapısını karakterize etmek için taramalı elektron mikroskobu (SEM) kullanılmıştır. SEM analizinin sonucunda darbeli elektro çöktürme ile piramidal büyüme elde edilmiştir. Yüksek frekans ve yüksek görev döngüsünde artan ortalama akım yoğunluğu ile daha küçük taneler ve daha az gözenekli yapılar tespit edilmiştir. Ortalama akım yoğunluğunun azalması ile tane yapısında düzensizlik gözlemlenmiştir. X-Işını kırınımı (XRD) analizine göre yüksek görev döngüsünde, yüksek frekansta ve yüksek ortalama akım yoğunluğunda daha küçük gümüş taneleri tespit edilmiştir. Darbe parametrelerinin gümüşün bakır taban malzemesi içine difüzyonu üzerindeki etkisi erke serpinimli spektroskopi (EDS) çizgi analizi ile analiz edilmiştir.

Anahtar Kelimeler: Darbeli Elektro Kaplama, Gümüş, Darbe Parametreleri, Anten, Dalga Kılavuzu

To My Family,

# ACKNOWLEDGEMENTS

# TABLE OF CONTENTS

# LIST OF TABLES

TABLES

# LIST OF FIGURES

FIGURES

xv

# CHAPTER 1

# INTRODUCTION

The silver is a chemical element in group 1B of the periodic chart. The silver, known as white metal among the people, has been used as jewelry for centuries [1]. However, it is a valuable element and important material for engineering applications other than as jewelry. It is a ductile metal, but it is harder than gold. It can be easily processed to form wire and sheet. For example, from 1 g silver, 2000 m wire can be drawn. There are two stable isotopes of Ag in nature. These are Ag-107 (51.8%) and Ag-109 (48.2%). There are also up to 14 radioactive isotopes which half-lives change between 4.5 seconds (Ag-114) and 40 days (Ag-105) [1]. It oxidizes easier than gold but more difficult than copper. It can easily react with ozone and sulfur in the air. However, silver oxides are not affected by oxygen and water. It does not erode by acids and some organic substances, but it can dissolve in nitric acid and concentrated sulfuric acid. The most well-known compounds of silver are silver oxide $Ag_2O$, silver sulfide $Ag_2S$, silver cyanide $AgCN$ and silver nitrate $AgNO_3$ [2]. Silver is more commonly used in plating compared to other materials. Silver is easy to use for many intents and purposes in the industry and it is basically difficult to replace by different metals. The other important mark is that it is the most economical valuable metal [1]. Compared to palladium and gold, silver has a price of one in twenty-five of the palladium and silver has a price of one in six of the gold. This takes the silver coating cost moderately low compared to other valuable elements [2].

Silver has impressive property having the most noteworthy electrical and thermal conductivity in addition to the reflectivity of light. Furthermore, it is one of the valuable metals having lighter weight (10.5 grams per cubic centimeters) and lower melting temperature (962 °C). The production of silver is relatively easy compared to

other metals. It is easy to alloy with metals such as aluminum and tin. These valuable properties of silver increase the usage especially in the microwave and RF industry day by day [4]. The high conductivity of silver reduces the loss of the highest microwave frequencies therefore silver can easily carry a high current load [6]. Therefore, reductions of the passive intermodulation levels of silver are possible with these properties. Additionally, it helps with diminishing the loss of RF signal and reducing the "Skin Effects" [7]. There is one potential disadvantage for utilizing silver plating in microwave parts, that is its propensity to build up an oxide film on the outside of the segment [5]. This occurs if the substrate is subjected to different substances, for example, sulfur, ozone or hydrogen sulfide. This problem is leveled out by a metal final finishing strategy called passivation. The metal oxide layer can be formed in a controlled manner to prevent oxidation. Covering the microwave/RF part with 100% pure silver also decreases the oxidation rate of silver. The most well-known problem in the silver coating is weakness of the coating [2]. However, silver coatings made on the base material, after the completion of all mechanical and thermal processes, prevents it from such incidents. The other undesirable properties of the silver coatings could be improved by optimizing the coating conditions.

Choosing the right base material is very important in many coating applications. The copper, nickel or their alloys can be selected as a base material. Since the adherence of silver to the aluminum for example is very low, base material firstly needs to be coated with one of the above metals and then silver can be plated [8]. Depending on the working conditions, an anti-tarnish coating can be made on the silver after plating [8]. However, silver coating conditions are the most important issues in the application of silver plating.

Silver can be applied both by direct current and by discrete and alternating pulse currents [3]. The pulse current can be the unipolar wave shape in which all current is in one direction or the anodic and cathodic pulses that can be mixed in bipolar wave shapes [9]. While only one parameter varies in direct current coating, more parameters

2

are variable in pulse coating. For example, these parameters are pulse current, pulse duration and pulse duty cycle. Pulse electrolytic coating has many advantages over direct current electrolytic coating [9]. Pulse electrolytic coating can change the pulse parameters to obtain the desired reduction speed, microstructure and composition. In the plating baths, the number of ions consumed relative to the regions with low current density is higher in the regions with high current density [9, 10]. When the current is turned off in the pulse electrolytic coating, the ions in the high concentration zone in the coating bath begin to migrate towards the areas where the concentration of the ions is reduced. When the pulse is switched on, the ion concentration distribution on the electrode surface will naturally become more homogenous. The accumulation on the coating pieces may also be more homogenous [10]. Because there is low metal ion concentration (first layer), the formation of secondary reactions (such as hydrogen reduction) will also decrease and the reduction efficiency will increase. Therefore; coating properties like electrical conductivity, hardness ductility, plating thickness distribution, grain size refinement and anti-tarnishing property can be optimized with pulse current coating [10].

Important restrictions in the direct current are rough deposits. These limitations result in problems especially in microwave/RF parts in the electronics industry where electrical conductivity changes by minor effects [11]. The effect of the pulse parameters on the surface roughness of the silver coating and on the S-parameter (scattering parameter) have been observed in this study. In the experiments, three parameters were selected for pulse silver plating. They were the duty cycle, frequency and the average current density. Three levels were selected for each parameter. The levels were 10%, 50% and 75% for the duty cycle; 10 Hz, 40 Hz and 80 Hz for the frequency and 0.5 A/dm$^2$, 1 A /dm$^2$ and 1.5 A/dm$^2$ for the average current density. The effects of their combinations have been observed in twenty-seven experiments determined from design of experiments application using Minitab software [12].

The aim of this study was analyzing the effects of pulse parameters on the surface properties of silver coatings of the copper base material in terms of surface roughness and S-parameter (scattering parameter). Grain refinement of the silver-plated material and smoother silver plating with finer grains were obtained as a result of this study.

# CHAPTER 2

# LITERATURE REVIEW

## 2.1. Horn Antennas and Waveguides

The horn antenna has a shape which is different from other reflector type antennas. This antenna is used in microwave and very/ultrahigh frequency range. Horn antenna is often used with waveguides. However, the waveguide can be used without the horn antenna [13]. The horn antenna can be used with waveguides to direct the wave of signal in a more efficient way. In fact, the horn antenna has an impedance harmony with the waveguide in an empty field. It is connected to the waveguide from the same interface [13]. The horn antennas prevent scattering of the signals in unwanted mode and provide a certain orientation to the waves. Since the horn antenna has a certain opening, it provides extra gain for transmission of waves. The length is also effective for the gain level [13]. The typical drawing of a microwave horn antenna is shown in Figure 2.1
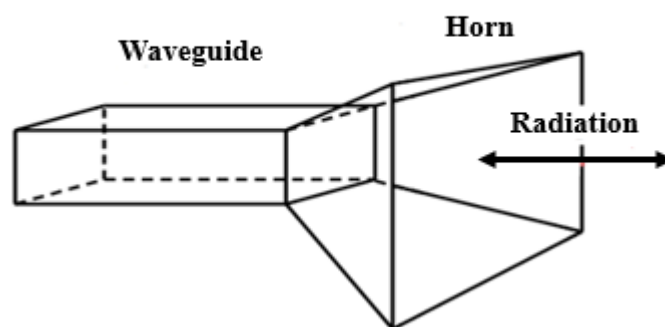
*Figure 2.1.* Schematic drawing of a microwave horn antenna

Pyramid, Sectoral, Conical, Exponential and Corrugated are various types of horn antenna. The most important feature of the horn antenna is the expansion angle. This angle can also be defined as flare angle. Even if horn antennas opening is rectangular or circular, the antennas have a certain angle [14]. This flare angle that affects the antenna gain and orientation is shown in Figure 2.2.
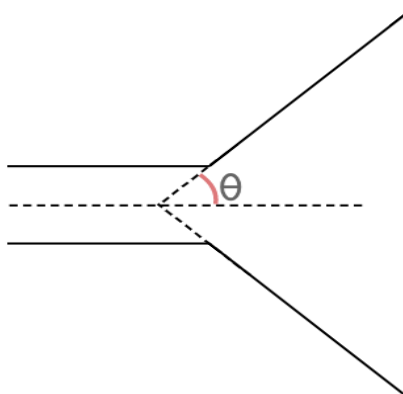


*Figure 2.2.* Flare angle of a horn antenna

For figuring out radiation of antenna, a basic theory and statement can be used. When the current starts, the signal waves move towards the horn antenna opening. The waves act as spherical wave shapes having a point called the phase center of the horn antenna [15]. As the phase in the horn antenna is spherical, a proper increase of the phase from the edges to the center occurs. A phase difference will be observed between the center point and the edges. This difference is called as a phase error. When this phase error increases, the gain decreases. Horn antennas have a wider beam width due to their structure.

The basic theory indicates that the horn antennas increases the wavelengths of various sizes when the electrical magnitude of the antenna increases. This increases the phase error [13]. A longer horn is used to obtain a narrow beam width. This narrow beam

width is achieved by a smaller flare angle. Therefore, phase error problems can be limited with using longer antennas [13]. When the horn antennas become bigger, they can reach high gain levels. In fact, the gain is related to the frequency. When the frequency increases, the gain and wave's orientation increase. In other words, the frequency causes to increase the number of the wavelengths. Some tables and graphs can be found in handbooks for antenna that show the best dimension and structure for the horn antenna. However, optimum geometry can be found for only a single frequency.

### 2.1.1. Horn Antenna Gain

The gain of the horn antenna can be easily calculated with several parameters. The gains of pyramidal and conical antennas which radiating equally in all directions are given in Equations 1 and 2 [16].

For a Pyramidal horn:

$$Gain = \frac{4\pi A e_A}{\lambda^2} \qquad (1)$$

For a Conical horn:

$$Gain = (\frac{\pi d}{\lambda})^2 e_A \qquad (2)$$

A: The aperture area

d: Conical horn aperture diameter

λ: The wavelength

$e_A$: Aperture efficiency ranging from one to zero

The aperture efficiency is directly related to the conductivity of horn antenna surface. Electronic conductivity is a parameter that exhibits the free-electron transportation ability of a material.

The radiation efficiency of reflector type antenna and insertion loss of waveguide transmission lines are directly related to the conductivity of the materials used to construct such structures. Signal quality of antennas and waveguides in the transmission of electromagnetic waves are also very much dependent on the surface finish that has good conductivity [17]. The inner surface of waveguides and horn antennas should be conductive. When the current is transmitted, it is dispersed from the inner surface. The high current scatters from the surface with a certain wavelength. The smoother the surface causes the higher the surface conductivity and the less the surface current loss. The homogeneous current distribution depends on the surface smoothness. It is known that metals with high surface roughness degrade the propagation of electromagnetic waves severely. So, performances of these antennas are strongly related with surface quality [17].

### 2.1.2. Material Selection for Horn Antennas

The increase in the number of metallic alloys and designs of composites for antennas and waveguides increase the chance of finding the optimum material. In general, regardless of which material selected, the surface which the current is transmitted in the antenna and the surface where the waves are formed must be conductive [16]. Generally, copper, aluminum, brass, gold and silver are good antenna materials. But nowadays, plastic and composite materials which are produced with easy production methods are being started to use in antenna applications [18]. Yet, electronic engineers prefer metals which can be easily processed. Copper is usually used for production of smaller horn antennas since it is a dense and conductive material [18]. Aluminum is also rapidly oxidized despite processed easily.

The choice of coating material in the antenna is very important as it can improve performance. Whatever coating is used, the surface of the horn to be coated must be physically smooth. Silver and gold plating are usually preferred because they are

generally good conductors [19]. The conductivity of various metals is given in the Table 2.1 [19].

Table 2.1. *The relative electrical conductivity of various metals*

| Metal | Relative Conductivity in 20°C (S/m) |
|---|---|
| Aluminum(pure) | 59 |
| Aluminum(alloys) | |
| Soft-annealed | 45-50 |
| Heat-treated | 30-45 |
| Brass | 28 |
| Copper | |
| Hard drawn | 89.5 |
| Annealed | 100 |
| Gold | 65 |
| Cast iron | 2-12 |
| Nickel | 12-16 |
| Phosphor bronze | 36 |
| Silver | 106 |
| Steel | 3-15 |
| Tin | 13 |

### 2.1.3. Plating of Horn Antennas

The reasons of using plating for antenna products are listed below:

•       Obtaining higher surface hardness

•       Obtaining higher electrical conductivity

•       Obtaining cost effectiveness

- Establishing better electrical contact between conductors

- Increasing corrosion resistance

- Obtaining thinner coatings and better surface quality

The coating thickness and roughness profile of the horn antenna in edge and buckling regions should not vary too much. This is the most important factor for evaluating the coating quality. Coating hardness is another important criterion for good quality. Gold, silver, nickel, copper and lead alloys are the most commonly used plating materials for horn antennas and waveguides. Palladium and white bronze are also used [20].

Silver is often used for soldering and brazing of RF and microwave components, like antennas and waveguides. Silver is a very good conductor. This means that the return loss is very low when it carries current at the highest frequencies. This coating can be advantageous especially for waveguides and antennas working at high frequency. The only disadvantage is that if there are ozone, oxygen-sulfur and sulfur in the environment, silver can be oxidized very fast. Passivation must be performed to prevent or slow down this rapid oxidation [20].

## 2.1.4. Skin Effect

The effect of the skin depth is observed in the materials which have electrical conductivity. This effect is the condensation of current on the outer surfaces. The current is distributed homogeneously at DC voltages. But at AC voltages, the skin effect occurs and increases with frequency. In fact, as the frequency increases at AC voltage, current moves from the center towards the surface [21].

In Figure 2.3, the balls show the distribution of the current on the surface. For example, when using a solid circular wire, the current does not flow through the inner face as the current will be emitted on outer the surface. So, this circular wire can be replaced by a hollow wire. Skin depth (μm) is given in Equation 3 [21].
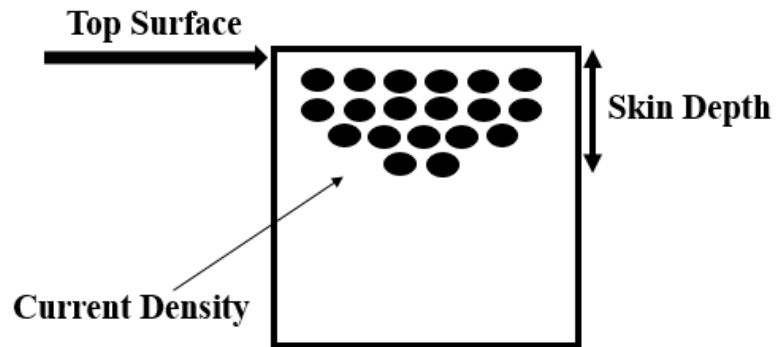
*Figure 2.3.* Schematic figure of skin depth

$$\delta = \frac{1}{\sqrt{f\,\mu\pi\sigma}} \qquad (3)$$

δ: Skin depth (μm)

f: The frequency (Hz)

σ: The conductivity (in mho/m)

μ: The permeability $4\pi \times 10^{-7}$ H/m

According to Equation 3, the skin depth decreases as the frequency increases. When the conductivity increases, skin depth also decreases. One of the reasons for the silver coating to be used effectively in the horn antenna and waveguides is that the depth of the skin is very low. Silver is a better conductor than copper and can be applied as a very thin layer (0.13-0.30 μm). Since conductivity of silver is very high, the skin depth will be reduced, and the RF current will use smaller part of the whole conductor [22].

### 2.1.5. The S-Parameters (Scattering Parameters)

The S-parameters are the electrically input and output relationship between the ports. If it is thought to be two ports, the expression defined as S12 becomes the power

transferred from port 2 to port 1. Ports which are any of two places in the network analyzer, may be explained as anywhere delivering or getting voltage and current [23].

If there are port-1 and port-2,

S11 = The power flowing back from the first port

S22 = The reflecting power from the second port

S12 = Power transferred from port 2 to port 1

S21 = Power transferred from port 1 to port 2

A communication system has two radio stations (radio 1 and radio 2). So, radio terminals (parts that transmit power to the antennas) will have 2 ports. S11 will be the reflective part of the power that radio-1 tries to transmit to antenna-1. The most commonly used parameter is S11. The S11 represents how much power is returned from the antenna. It is also known as reflection coefficient or return loss. If S11 = 0 dB, this indicates that all the power is reflected. There are several parameters for the antenna shown in decibels. For example, antenna or waveguide gain is usually given in decibels. Decibel systems are used in cases where quantities vary greatly. In the case of Richter, where the earthquakes occur, decimals are like decibels, because the magnitudes of earthquakes can reach very high amplitudes which can be very high. As shown in Equation 4, decibel can be computed as 10 times of the logarithm of power rates measured power (P2) and a reference power (P1) [24].

$$\text{Rate of power (dB)} = 10 \log\left(\frac{P1}{P2}\right) \qquad (4)$$

## 2.2. Electrodeposition

A typical electrolytic cell form is shown in Figure 2.4. The electric current is indicated by "i". This current is carried by ions in the electrolyte. Electrodeposition is the process of collecting a material to another surface from an ionic solution. The solution contains

both positive and negatively charged ions. Cations, ions which are charged positively, are gone to the cathode which is charged negatively. On the contrary; the anions, ions which are charged negatively, are gone to the anode which is charged positively. The place of performing the reaction of deposition is the cathode. The current value which occurs at the cathode is related to the thickness of the coated surface. Therefore, the current density is called as the current which occurs per unit area [25]. Anode and cathode reactions are not interconnected [25]. Depending on the kinds and concentrations of ions, different reactions may occur at the cathode and anode. Each reaction at the electrodes has a certain voltage. The reaction which has the most positive voltage, one will be the reversible reaction of the corresponding electrode.
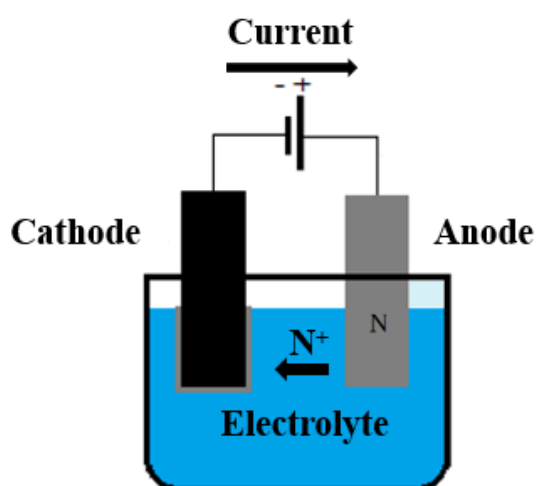


*Figure 2.4.* Electrolytic cell form

Water is the most commonly used solvent. Water dissolves and ionizes many salts. Non-aqueous solutions, molten salts, may also be used. However, these solutions are widely used in the production of sodium, magnesium and aluminum [26].

Generally, electroplating doesn't work at 100% cathode efficiency. The ratio of actual coated material over theoretically expected material according to the Faraday law is the cathode efficiency. The cathode efficiency is determined by considering the current efficiency. The cathode efficiency is how much of the given current is used for cathode deposition or anode removal.

Another important parameter is throwing power. It is the depth stability of a deposited material on chaotically figurate part. Leveling ability is the power of straightening an irregular surface with coating. Leveling is increased with supplement of leveling agents into the bath [27]. Brightening is the power to create a shiny fine structure after coating. This can be done with the addition of brighteners.

## 2.3. Thermodynamic Analysis of Electrochemical Reactions

Energy is input between the electrodes in the electrodeposition process. On the other hand, an electrical energy is produced from the galvanic cell. Chemical changes occur in the cell as a result of these energy exchange processes. There is a relationship between electrical energy and chemical changes. This relationship can be calculated from the second rule of thermodynamics. The thermodynamic analysis for the spontaneous reactions under constant T and P is shown in Equation 5 [28]:

$\Delta G < 0$

$\Delta G = \Delta H - T \Delta S$

$\Delta H = \Delta U + P \Delta V$ (under constant P)

From the fist law of thermodynamics:

$\Delta U = q - w$

Where $w = P \Delta V + w'$ (under constant P, w' is the work other than P-V type)

Replacing them in the $\Delta G$ equation

$\Delta G = q - P\Delta V - w' + P\Delta V - T \Delta S;$

$$\Delta G = q - w' - T \Delta S \qquad (5)$$

Where; q: Quantity of heat that flows into the system, $\Delta V$: Volume change of the system, $\Delta G$: Gibbs energy change of the system, $\Delta S$: Entropy change of the system, w': The electrical work in an electrochemical process, $\Delta U$: Internal energy change of the system [28].

The quantity of w' is linked on how the energy is reserved from the path [29]. Nearly all the emf are revealed as decreasing voltage throughout $R_{ext}$ and the maximum work will be done. These exists when $R_{ext} >> R_{int}$ the electrical charge passing rate is very low. In any case of generating heat in the electrolyte or interfaces of electrodes, the system temperature will not be different more than infinitesimally from the surroundings at these conditions. In addition, q (Heat transfer) is reversible [29]. The electrical work coming from the carrying current by the products and the electric potential difference (emf) can be found easily using Equation 5.

In Equation 6, F is the Faraday's constant and it is 96487 Coulombs/g equivalent. In this way 1-gram mole ion of n valance is carried through a voltage difference between the electrodes [28].

$$\Delta G = -w' = -n\,F\,E \qquad (6)$$

It can be seen that $\Delta G$ and E have opposite signs; spontaneous reactions in galvanic cells result in positive potentials, non-spontaneous reactions, requiring energy will have negative potentials.

## 2.4. Nernst Equation

The thermodynamic analysis of an electrochemical reaction could be summarized with a practical demonstration. A general electrochemical cell can be expressed as follows [30]:

- M, $E_B$| $B_{ox}$, $B_{red}$ || $A_{ox}$, $Ar_{ed}$| $E_A$, M +

$E_A$ and $E_B$ are two electrodes and they do not have to be the same metal. During the operation one of them is oxidized while the other is reduced. A boundary can be set

to separate these two electrodes. The twin lines ‖ at an intersection, point out that transfer of ions across the border occur. The reduction and oxidation members of pairs are related to any other of the reduction half-reactions [31].

$1/z_A (A_{ox} + n_A e- \longrightarrow A_{red}) E_A$

$1/z_B (B_{ox} + n_B e- \longrightarrow B_{red}) E_B$

$1/z_A A_{ox} + 1/z_A B_{red} \longrightarrow 1/z_A A_{red} + 1/z_A B_{ox} \qquad E = E_A - E_B,$

$E_A$ and $E_B$ are electrode potentials. $E°_A$ and $E°_B$ are the corresponding standard half-cell e.m.f of A and B. Gibbs energy change of cell process is;

$$\Delta G = \Delta G^0 + RT \ln Q$$
$$-nFE = -nFE° + RT \ln Q \qquad (7)$$

Q is the natural log of the reaction quotient at the moment in time. If an arrangement is made, an equation will be obtained as follows [31]:

$$E = E^0 - \frac{RT}{nF} \ln Q \qquad (8)$$

This Equation 8 shows behavior of electroactive species with respect to the standard potential $E^0$. In the Nernst equation, formula can be identified as base-log form and at $25^0C$.

$$E = E^0 - \frac{0.5915}{n} \log Q \qquad (9)$$

## 2.5. Polarization and Overpotential

There is a relationship between the amount of current passing through an electrochemical system and the electrochemical change. The Faraday law explains this relationship in Equation 10 [32].

$$m = \frac{MIt}{nF} \qquad (10)$$

m = Mass of the substance

M = Molecular weight of the substance

I = Current passed (A)

t = Time for which current passed (s)

n = Number of electrons transferred

F = Faraday constant (96487 C/eqv)

All Faradaic processes contain transferring of electrons on the interface of electrodes or electrode itself. There is an equilibrium potential of the Faradaic processes. This potential depends on the free energy of the reaction. Polarization is a phenomenon that adversely affects the performance. This causes the electrode potential to shift from the equilibrium value when the electric current passes through a galvanic cell [32]. This shifting from the equilibrium value is called polarization. So, the overpotential is the distinction of the potential between the realized voltage under working conditions and the theoretical voltage. Formula of the overpotential is shown in Equation 11 [32].

$$\eta = E - E_{eq} \qquad (11)$$

$\eta$= Overpotential

E= The resultant potential

$E_{eq}$= Equilibrium potential

The overpotential influences the cell potential [32]. This is shown in Figure 2.5 [32]. There is an optimal galvanic potential in terms of thermodynamics. This occurred by the differences of reduction potentials of the two half cells. The same correlation can be considered for electrolytic cells. The required electrode potential or the observed potential is different from the optimal value. The reason is that the galvanic potential

is less than the theoretical value or the electrolysis potential is higher than the theoretical value.

Electrolytic and galvanic cells are opposite in terms of the overpotential. For example, in an electrolytic cell, more energy is needed than the required thermodynamic value to perform the redox reaction. However, the galvanic cell will have less energy than its thermodynamic value [32]. If there was no polarization, the reaction rates at the anode and cathode would be equal. As the potential increases, the anode acts more anodic and the cathode acts more cathodic. When the deposition reaction accelerates, the dissolution reaction slows down. So, in fact, polarization voltage and overvoltage are the potential change in both electrodes. Overvoltage at the cathode is indicated as negative while that at anode is indicated as positive sign [32].
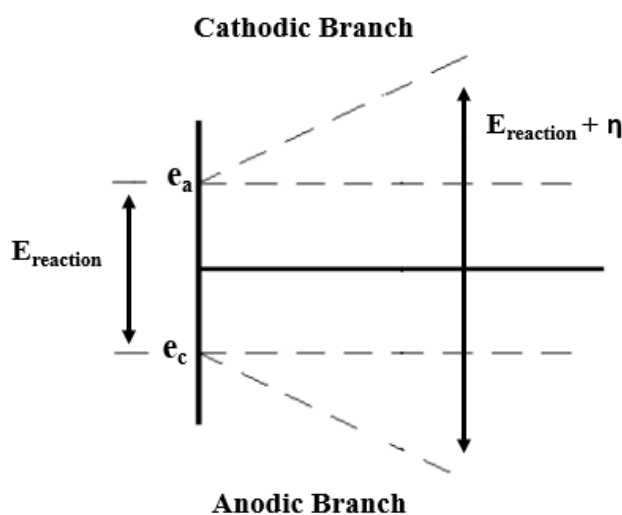


*Figure 2.5.* The overpotential formation

Current density vs voltage curve of cathode relative to a reference is shown in Figure 2.6 [33]. Current is zero up to the point A. There is no electrode reaction until the voltage is increased to A. However, the ions are ready to accumulate near the electrode. But the electrode reaction does not take place immediately when the current

18

flows. Additional increase must be done to the current for reaction to commence. When the current increase continues, the voltage rises to where the reaction starts, in Figure 2.6 [33], the electrode reaction begins at point B. Resistance to the polarization is explained as the potential difference between A and B.
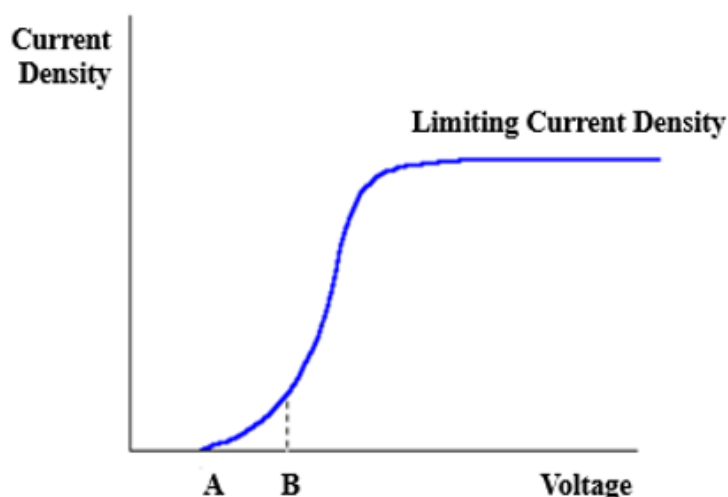


*Figure 2.6.* Current density versus voltage curve

The activation and concentration overpotentials are the two kinds of the overpotentials. The rate limiting of the reaction step is related to the activation energy barrier [34] for activation overpotential. Activation polarization is considerable for oxidation. Concentration overvoltage is important in reducing reactions. The ions around the cathode are reduced while the electrodeposition is continuing. This situation decreases the reversible potential due to the decrease of ion in concentrations. A schematic diagram of the current density and electrode potentials of anode and cathode reactions are shown in Figure 2.7 [34]. This belongs to electrowinning of a metal M. As seen from the graph, the positive side is the anode and negative side is the cathode. The point where the deviation begins is starting point for overpotential. As current density increases, the anode will be more positive, and the cathode will be

more negative. The applied potential determines the energy to be used for electrowinning of M. In addition, energy consumption is also very important for electroplating. Electrode design, cell design and operating conditions are adjusted to optimize energy consumption in electrolytic processes.
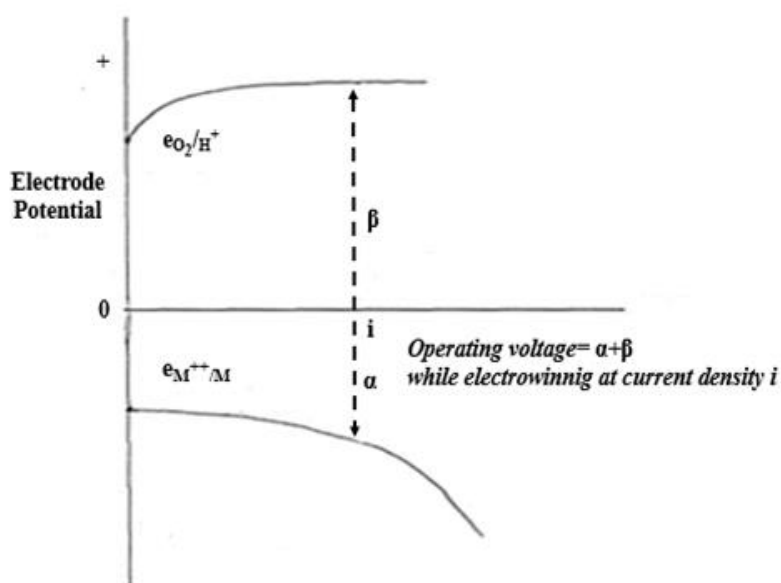


*Figure 2.7.* The electrode potential versus current density

## 2.6. Silver Electroplating

Electrolytically plated silver is used for the coating of aircraft bearings, numerous radar components and electronic components [34]. The silver coating is also made for good reflection of electromagnetic waves. At 100% cathode yield, it is necessary to charge 2.67 ampere-hour for 100-micron silver on a 1 dm² metal surface. In a 100% cathode yield, 4.025 g of silver can be applied with each ampere-hour of electricity passing through the silver coating solution. The average yield of cyanide type silver baths changes between 96% and 98% [35]. When the yield is taken as approximately 97%, this means that the coating of 3.90 g silver per ampere hour can be done. Silver is a precious metal. This means that it can be coated on the nonprecious metals like

brass, copper, iron and their alloys by immersing [36]. Accordingly, it would not be wise to plate silver directly onto the base metal as the silver plated with dip operation will cause a weak adhesion to the entire silver coating. Therefore, in commercial applications, two types of silver-plating solution are used to make silver coating. The first solution is called flash (strike) solution. The silver concentration is very low in this solution. When a piece is immersed in this solution for coating, there will be so little silver in the environment that the silver is drenched or not coated at all [37]. When current passes through the solution, a small amount of silver is coated on the material. The second solution is the normal silver coating solution. This bath contains silver in its normal coating concentration. The thick silver sheets can be coated on the piece in this bath.

In the silver-plating process, an aqueous solution of a silver salt is present. Conductivity is provided by passing the current between the anode and the cathode. The silver ions are dissolved from the anode and deposited on the cathode. The hydrogen evolution may also take place at the cathode. The schematic diagram of silver electrodeposition of a spoon is shown Figure 2.8 [38].
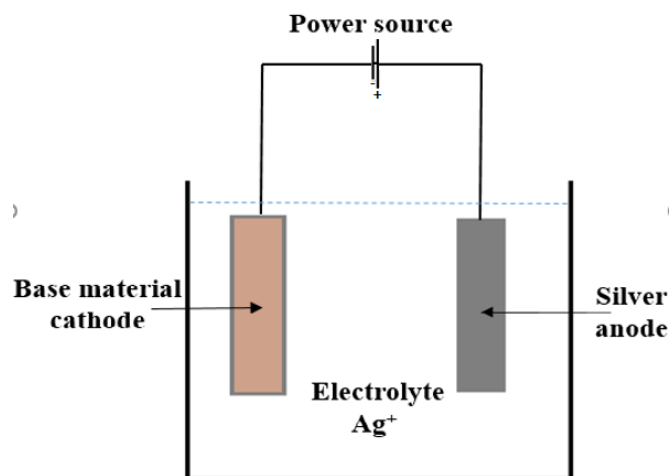


*Figure 2.8.* Schematic diagram of silver electrodeposition

The electrode reactions are;

Oxidation reaction at Anode: Ag(s) → Ag+(aq) + e-

Reduction reaction at Cathode: Ag+(aq) + e- → Ag(s)

### 2.6.1. Silver Plating Baths

The silver coating bath can vary depending on the surface to be coated, the silver property and the area to be coated. For example, a high-density silver bath is used for thick coatings in engineering applications. But in decorative applications, baths containing less dense silver are used. When the silver density increases, it can be operated at high current density, so the coating deposition rate increases.

The contents of baths are given in Table 2.2 [37]. $KAg(CN)_2$ is a compound that is formed by alkali metal and silver cyanide. KCN and AgCN are mixed for the formation of this compound in industrial practice. For small laboratory and other applications, the solutions are prepared directly with potassium silver cyanide [38].

Table 2.2. *Ranges of add-ons of silver baths*

|  | For Thinner Applications (g/L) | For Thicker Applications (g/L) |
|---|---|---|
| Silver (as metal) | 20-45 | 40-120 |
| Silver cyanide | 31-56 | 45-155 |
| Potassium cyanide (total) | 50-78 | 70-230 |
| Free potassium cyanide | 35-50 | 50-165 |
| Potassium carbonate | 15-90 | 20-95 |
| Potassium nitrate | ---- | 45-65 |
| Potassium hydroxide | ---- | 5-30 |
| Current density, $A/dm^2$ | 0.5-1.5 | 1-10 |
| Temperature, °C | 20-28 | 38-50 |

The silver, which is deposited on the coating surface, i.e. the cathode, comes from potassium silver cyanide. There is always an optimum value between cyanide and silver. When the silver ratio drops and the rate of free cyanide increases, the throwing power can be increased. High concentration means high current density. Lower silver content baths are used for 2-5-micron coatings [38]. Alkali cyanide has various contributions. Alkali cyanide increases conductivity, enhances cathode polarization and promotes silver complex ion formation. Sodium cyanide is not commonly used. Potassium cyanide is more preferred. The main reason for this preference is good conductivity, increased solubility of potassium carbonate and increased limiting current density.

Another additive is potassium carbonate. This additive also improves conductivity. It also increases the throwing power. The main reason for this increase is the higher anode and cathode polarization. A minimum amount of potassium carbonate may be added to the solution initially. It can be added up to the maximum amount specified in Table 2.2 together with the decomposition of cyanide [38]. Potassium carbonate balance is also important. Very high values of potassium carbonate must not be added. Rough coatings and deposits are obtained at high values. The specified ranges should be used.

Potassium nitrate may be preferred to obtain fast plating. Using 40 to 60 grams per liter reduces free cyanide and accelerates dissolution of the anode. Hydroxides can also provide similar additional properties to the solution like as potassium nitrate. Phosphates, chlorides, borates etc. can be added for additional good properties. To illustrate, silver hardness can be enhanced with these additions.

Additional inserts can be used to achieve high gloss silver finishes. Antimony, bismuth, selenium and sulfur-containing compounds can be used for good gloss. Organic brighteners are usually used in silver plating baths but activating functionality comes from sulfur content. The primary brightener is used for high gloss silver

finishes. A surface-active agent is used secondly. The second one allows adsorbing the first polisher to the surface in a specific direction.

Only two of the non-cyanide silver-plating baths have achieved success. First one contains organosilver structure with well-known succinimide. The second one contains alkaline thiosulfate with succinimide as an anode corrosion initiator. Generally, silver coating baths that are prepared fresh are better than aged (used) baths. Therefore, it is sometimes wise to clean the baths [38].

## 2.6.2. Anodes

Pure silver anodes having higher than 99.5% purity should be used while operating a silver-plating bath (not flash). Anode and the cathode surface area ratio should be 1:1. The average current density of the anodes should not be higher than 1.6 A/dm² for normal bath. But it should be 4.3 A/dm² for the high-speed orifice baths. The currents that exceed this speed can cause darkening of the anode. There is an occasional problem associated with silver anodes. This problem is surface fragmentation. Falling particles from anode can make metal useless and cause rough coating. Platinized titanium anode can also be used as an anode material. This provides some advantages such as long bath life, constant anode geometry, energy saving and low maintenance.

## 2.7. Pulse Electrodeposition

The coatings that are applied using pulse current have increased in the last thirty years. These coatings are used widely in the semiconductors, amorphous coatings, composite coatings and anodizing with developments of the pulsed electrodeposition. Although the pulsed current is primarily used in the electronics industry, the benefits of this technique have been used in different industries. Electrochemistry is one of the examples of this usage. The current is given by changing between different values in the case of pulse electro-plating. The lower value of the variable current here is

generally zero. Pulses have equivalent amplitude, period and polarity are discrete with zero current. Each pulse has the time when the current is applied ($t_{on}$) and the current is not applied ($t_{off}$). The sum of the times which the current is given, and the current is not given mean one period. This is also indicated in Figure 2.9. [39, 40].
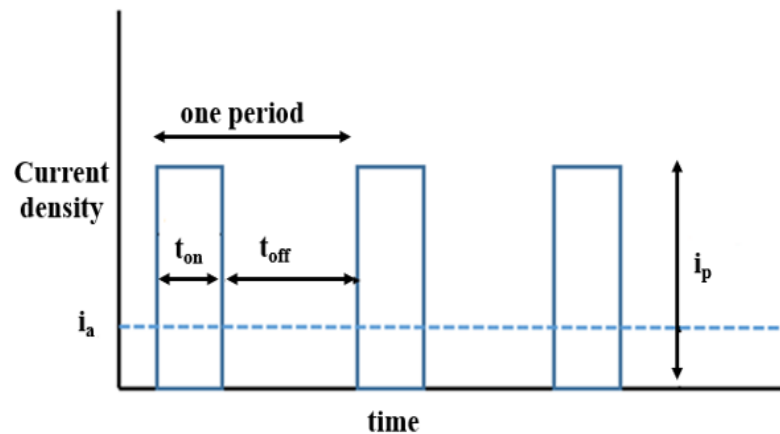


*Figure 2.9.* Waveform of typical pulse current

The average current density is shown as $i_a$ and peak current density is shown as $i_p$. It is possible to change the pulse amplitude and width. These changes cause controlling the film structure of deposition and atomic order thickness [41]. This is very important because grain nucleation is accelerated, and more grain formation occurs in the coated material. The number of grains per unit area increases by pulsed electrodeposition. In addition, the coating properties such as coating hardness and current efficiency can be improved as a result of finer grain structure [42]. It is not possible to control such grain structures in the traditional DC coating. It is also possible to obtain even smooth and homogeneous surfaces because of the improved grain structure in the pulsed current deposition. There is no restriction for programming of the applied current waveform in the modern electronics and microprocessor. Therefore, this ability of the electronics industry may be implemented to coating industry to attain feature demands [41].

Waveforms have two groups. The first one is unipolar which means that there is no deviation in the direction of pulses. The second one is bipolar which can be defined by using anodic and cathodic pulses together. Moreover, there are too many variables for the waveform. Variable numbers increase when waveform becomes complex [43]. Typical waveforms are shown in Figure 2.10 [39].
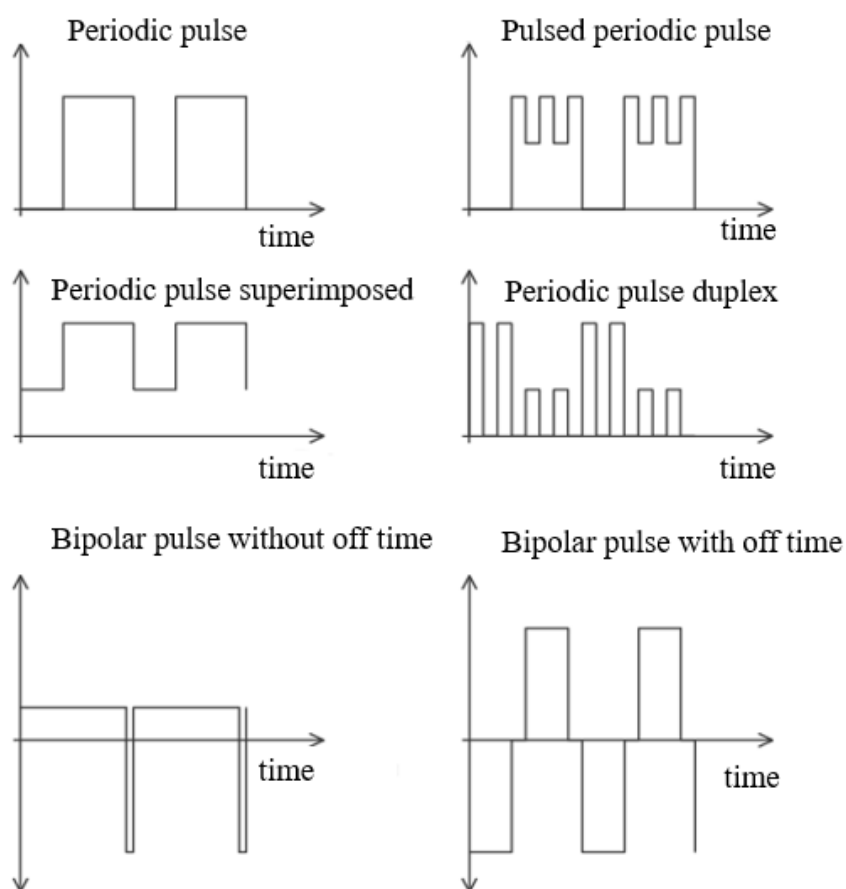


*Figure 2.10.* Typical waveforms

### 2.7.1. Advantages of Pulse Electroplating

A negatively charged layer is formed around the cathode during electroplating. It is not possible to thicken the skin layer of coating made with conventional direct current when it reaches a certain thickness. One of the main reasons of not achieving higher thicknesses is that it is not possible to reduce the hydrogen overpotential in conventional coatings. The consumption of ions in the bath is proportional to the current density. When the current is switched off, ions can homogenize in the solution by scattering to the descending regions. When the current is increased, the homogenized ions will be used for re-coating [41].

The number of parameters that can be changed in the pulse coating is more compared to direct current coating. For example, $t_{on}$, $t_{off}$, frequency and duty cycle can be changed. Only current and voltage which are dependent on each other can be changed in DC coating. There are some advantages of changing more parameters in pulse electroplating [10, 39]:

- The limiting current density increases while doing pulse electrodeposition. The reason is the loading of metal ions in the diffusion layer during off time ($t_{off}$) of pulse electrodeposition.
- The most important advantage of pulse electrodeposition is obtaining the desired grain size, composition and hydrogen contents by changing the pulse parameters.
- Compared to the direct current coating, the need for additives is greatly reduced in the case of electrodeposition made by pulsed current.
- Residues that occur in high current density areas can be reduced in pulsed coatings

### 2.7.2. Pulse Current Coating Parameters and Effects

There are three basic parameters in pulsed current coating. These are on-time, off-time and peak current density. Frequency, duty cycle and average current density are derived from these three basic parameters as given in equation 12, 13 and 14 [44].

$$Frequency = \frac{1}{t_{on} + t_{off}} \qquad (12)$$

$$Duty \; cycle = \frac{t_{on}}{t_{on} + t_{off}} \qquad (13)$$

$$i_a = i_p * duty \; cycle \qquad (14)$$

Where $i_p$ is the peak current density and $i_a$ is the average current density. The average current density, peak current density, $t_{on}$ and $t_{off}$ are shown in Figure 2.9.

The morphology of coatings can be affected by mass transport. In addition to this, the mass transport is also crucial in terms of limiting the deposition rate and throwing power (macro & micro). Limiting current density, $i_L$, is the crucial factor of pulse current plating for mass transport. Limiting current density is related to the on time of pulse plating. When the extended-on time occur, it is expected that the value of limiting current density becomes smaller. The on time of the pulse plating must be low to make applied current density remain under limiting current density. On the contrary, it should be long enough to charge the double layer. So, there is an optimum value for the on time. The limiting current density of pulse current can be higher than the limiting current density of direct current. When the average current density is lower than the limiting current density of direct current and the peak current density is lower than the limiting current density of pulse current, the dendritic structure is disrupted, and a compact structure is obtained. Powder deposits form near the limiting current density is occurred in the case of direct current coatings. In the case of direct current coatings, dust deposits can form near the limiting current density [40]. If there

is a small diffusion layer, smooth deposits can be observed in pulse electroplating. This condition occurs even if working near limiting current density.

Crystallization is the union of atoms or ions. The new crystals are formed and built on previously formed crystals. This crystallization event is highly influenced by the atom population, the overpotential and the diffusion rate of the surface. More atomic population and high overpotential can be achieved at high peak current density. The nucleation rate and the atomic population increase with high peak current density during on-time of pulse electrodeposition. In fact, the basic principle here is the changing of electro crystallization mechanism by pulse electrodeposition. Therefore, the physical and mechanical properties of the metal formed will change [45].

The rate of nuclei formation ($v$) is given in Equation 15.

$$v = K1e^{\left(\frac{-K2}{|\eta|}\right)} \qquad (15)$$

Constant of proportionality is termed as *K1*. The crystallization overpotential is termed as $\eta$. Peak current density is *K2*. Equation 15 may indicate that nucleation and overpotential are increased when peak current density is increased. Deduction of current throughout off time fosters re-nucleation rate because of impurity desorption [45]. When the duty cycle increases, the current on time ($t_{on}$) also increases as shown from the duty cycle formula in Equation 13. When duty cycle is reduced, peak current density can be applied for smaller period. Therefore, less deposition is observed [45]. If the frequency and duty cycle are reduced, the peak current density is also reduced and so the thickness of the coating decreases accordingly. In fact, while observing that the effect of frequency and duty cycle parameters on the thickness of the coating, the current efficiency should also be considered. Although a linear effect in terms of increasing and decreasing of current efficiency may be expected, parameters of pulse electrodeposition have an optimum point on current efficiency [45]. As can be seen from Figure 2.11, the increase of duty cycle after a certain value decreases the current efficiency rather than increasing it [46]. This behavior may be attributed to hydrogen

formation reaction at the cathode after a certain duty cycle value during silver electrodeposition.

In order to observe the effects of pulse parameters in pulse electroplating applications, various studies have been conducted for nickel, gold and copper coatings which are widely used in industry.

Balasubramanian et al. [47] mention the effect of pulse parameter on pulsed electrodeposition of copper. In that study, a solution that are made up of $CuSO_4.5H_2O$ and $H_2SO_4$ was used. Firstly, the strike solution of copper that was used for plating of copper which has thickness of 2 µm was used with solution consisting of cupric chloride and HCl. Cu coating which has good adhesion on stainless steel were electrodeposited. Pulse coatings were analyzed at room temperature using different duty cycle and different frequencies. It has been determined that different duty cycle and different frequencies change the current efficiency and coating thickness. Average current density was kept constant at 4 A/dm$^2$. Maximum thickness and current efficiency were obtained at 80% duty cycle and 50 Hz.

S. Benhenda et al. [48] has conducted studies to observe the electrical contact behavior of pulse coated nickel plating. In this study, an additives-free Watts bath was used. Solution contains only $NiSO_4.6H_2O$, $NiCl_2.6H_2O$ and $H_3BO_3$. This study is important to determine the effects of pulse parameters on electrical properties. No additives were made to the coating bath in this study. Nickel plating was made on copper by using direct and pulsed currents. As a result of the study, it was observed that preferred crystal orientation changes with current density and frequency. (111) orientation was interrelated to porosity and roughness of the structure. According to the study, the resistance of nickel plating was claimed to be related with surface topography and surface hardness. In addition, it has been determined that the growth morphology in pulsed current changes according to toff and ton parameters. Smoother and denser surfaces were obtained at high duty cycles. The contact resistance was lower on these surfaces. Less porosities and homogeneous coatings were formed at 2 A/dm$^2$ current

density and 50 Hz frequency. As a result of the study, it was claimed that pulse coatings are exposed to less corrosion. It is stated that the studies were carried out at room temperature and glossy surfaces were obtained in pulse coatings even at room temperature.

M. Sajjadnejad et al. [49] also mentioned XRD and SEM characterizations of pure nickel coatings on copper substrates under pulse conditions. In this study, a solution containing nickel sulfate was used. Nickel sulfate is useful because of easily soluble, easily trading and low-cost. The effects of frequency, duty cycle and current density in terms of crystallographic orientation, microhardness and morphology of surfaces were analyzed. It was stated that nickel deposits crystallite size is higher at high duty cycle and current density. The crystal orientation regularly altered from randomly oriented texture at 1 A/dm$^2$ to texture of (200) at 10 A/dm$^2$. Texture coefficient and (111) peak intensity reflection increased at high pulse frequencies. Peak intensity of (311) increased with increasing duty cycle. (111) texture evolves the deposits' microhardness. However, nickel deposits having (200) texture were ductile. Deposits acquired at high duty cycle and current densities showed a combined morphology of large and small grain structures. The highest microhardness was reached at duty cycle of 50%, frequency of 10 Hz and average current density of 4 A/dm$^2$. This maximum microhardness was 193 HV. In this thesis about silver plating, small grain structures were obtained at high current cycle and high duty cycle.

C. J. Stimetz and J. J. Hren mentioned [50] the pulse electrodeposition of gold. In this study hard gold plating solution was used. This solution consists of cobalt salt. A semi-bright and compact deposition occurred at a current density of 0.3 A/dm$^2$ and a duty cycle of 10% in this study. The studies were carried out at direct current at 0.8 and 1.2 A/dm$^2$ current density and 50% duty cycle at pulse current. This study showed that decreasing the duty cycle at these current densities causes formation of rounded, nodular topology and matte deposits. There was no significant difference between conventional and pulse current coated gold deposits at low current density and high duty cycles as concluded from the results of TEM and electron diffraction analyzes.

In this study, the sizes of gold grains were distributed between 12 nm and 60 nm. The grain sizes were distributed to smaller values by pulse plating. There was a distinction of growth twin density in the deposits of pulse electroplated structure at the 50% duty cycles compared to the others which were conventional plating. In literature, it is known that these twins have mechanical, physical and electrical importance. However, no analysis was made in this study. Crystals between 5 to 10 nm diameters showed equal distribution in samples. The indexed electron diffraction patterns for these DC and pulsed plated cobalt hardened alloys indicated an fcc crystal structure. This is a useful study to demonstrate the grain difference between conventional and pulse plating for gold plating.

### 2.7.3. Effects of Pulse Plating Parameters on Silver Coatings

C. Shanthi et al. [46] studied about particles size, hardness, and tendency to tarnish and surface properties on pulse silver coating. An alkali cyanide bath was used in this study. Average current densities of 1 $A/dm^2$ and 9.3 $A/dm^2$ were selected. The silver coatings were performed to determine the effects of high and low duty cycle and frequency differences on the properties of coatings. As a result of this study, it has been observed that the frequency and duty cycle affect the hardness of silver deposits and the current efficiency of the coating process. Finer grains were achieved at low peak current density and high duty cycle. Best quality silver plating was obtained at 10 Hz frequency, 60% duty cycle and 3.13 $A/dm^2$ peak current density. The worst quality silver plating was obtained at higher peak current densities. In addition, the fastest tarnishing property was obtained at 10 Hz frequency, 20% duty cycle and 9.3633 $A/dm^2$ peak current density.

When the duty cycle increases, the current on time ($t_{on}$) also increases as shown from the duty cycle formula in Equation 13. When duty cycle is reduced, peak current density can be applied for smaller period. Therefore, less deposition is observed [45].

If the frequency and duty cycle are reduced, the peak current density is also reduced and so the thickness of the coating decreases accordingly. In fact, while observing that the effect of frequency and duty cycle parameters on the thickness of the coating, the current efficiency should also be considered. Although a linear effect in terms of increasing and decreasing of current efficiency may be expected, parameters of pulse electrodeposition have an optimum point on current efficiency [45]. As can be seen from Figure 2.11, the increase of duty cycle after a certain value decreases the current efficiency rather than increasing it [46]. This behavior may be attributed to hydrogen formation reaction at the cathode after a certain duty cycle value during silver electrodeposition.



*Figure 2.11.* Effect of duty cycle on current efficiency during pulse current silver deposition [46]

Although there are earlier studies on roughness [45, 46], the effect of pulsed silver-plating parameters on return loss (S11) was not examined previously. In addition, the effects of these parameters on the diffusion of silver atoms to the plated structure were not examined in the previous studies.

# CHAPTER 3

# EXPERIMENTAL PROCEDURE

## 3.1. Preparation of Electroplating Solution

The types of silver cyanide coating baths may vary depending on the properties of the desired silver coating. A typical cell used during silver electroplating can be seen elsewhere [51]. Additions in the electrolyte can change brightness and color of the silver to be coated. There are also commercial silver plating solutions available. But most of academic studies use solutions that are obtained by adding a certain amount of salts and other components to pure water.

Only silver potassium cyanide, potassium cyanide and potassium carbonate salts were used in this study. No organic compounds were added to the solution to enhance the brightness because, the functional part of the waveguide is the inner surfaces that are coated with conductive material. Outside surface can be painted so the appearance of the coating in these systems is not very important. To increase conductivity of the electrolyte, potassium carbonate was incorporated to this solution. This addition increases anode and cathode polarizations, also it helps increasing throwing power. An electrolyte that consists of 45 g/L silver cyanide, 75 g/L potassium cyanide and 25 g/L potassium carbonate was developed. A 250 ml beaker was used for each experiment and 200 ml solutions were prepared for this beaker [52]. The samples were immersed into the water immediately after coating to avoid contact with air. Anti-tarnishing operation was applied to the samples to prevent atmospheric attacks after removing them from water [53]. Umicore anti-tarnish 616 was used to obtain protective layer in this study [53]. This anti-tarnish forms a protective coating of a few nanometer thickness and protects it from oxidation and discoloration. All the coating experiments were carried out at room temperature.

## 3.2. Efficiency Calculations

Prior to the experiments which were designed to study the effects of pulse parameters, efficiency calculations were made. Measurements were taken from three tests by employing the parameters shown in the Table 3.1. 9 µm thickness was targeted for plating. The measured thickness values are also given in Table 3.1. These thickness values were found with using combined XRD and XRF Spectrometer. The average coating thickness of three samples was measured as 7.93 µm. Therefore, experiments were performed with an average efficiency of 88%. Test durations were calculated by using this efficiency in the experiments that follow.

Table 3.1. *Efficiency results of experiments*

| Duty Cycle % | Frequency (Hz) | Average Current Density (A/dm²) | Peak Current Density (A/dm²) | Pulse on Time (ms) | Pulse off Time (ms) | Time for 9µm Thickness (min) | Thickness (µm) |
|---|---|---|---|---|---|---|---|
| 80 | 100 | 1.8 | 2.3 | 8 | 2 | 17.2 | 7.7 |
| 60 | 50 | 1.3 | 2.2 | 12 | 8 | 24.1 | 7.9 |
| 20 | 25 | 0.8 | 4.1 | 8 | 32 | 40.2 | 8.1 |

## 3.3. Preparation of Anode, Cathode and Plating Equipment

The purity of copper coupons, which was the substrate material of pulse silver plating, was 99.9% in these experiments. Coupons were cut to size of 28.5X40X2 mm from a copper sheet. Images of sample coupons before and after silver plating are shown in Figure 3.1.
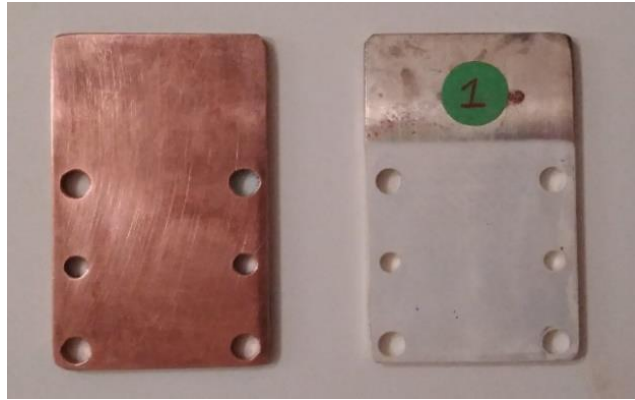
*Figure 3.1.* Images of copper coupons before and after silver plating

While measuring the scattering parameters from the coupons, 2 mm holes were necessary from four corners of each coupon to place them properly to the device that is used to measure the scattering. An end-launch adapter which was connected to the network analyzer was used for the measurements. The coupons were perforated from their corners to make it fit the test setup since a test device suitable for wr90 waveguide dimensions were installed [54]. Sanding process was done with 600-800-1000-1200-2000 grits respectively over each coupon for bringing each coupon to similar roughness value before coating. Then, each coupon was brought to mirror brightness appearance using automatic polishing machine employing 0.25 μm diamond polishing paste and rotating felt discs.

Commercially available meshed platinized titanium was used as anode material. Because this anode material has low weight, excellent conductivity and high current efficiency in silver plating solutions. Furthermore, it is inert and insoluble in the cyanide solution. A square anode of 3 cm$^2$ was cut to accommodate 250 ml beakers. In the experiments, Keysight (formerly Agilent) B2912A low noise power source, which can give both pulse and direct currents, was used. A picture of the test set-up is shown in the following Figure 3.2.
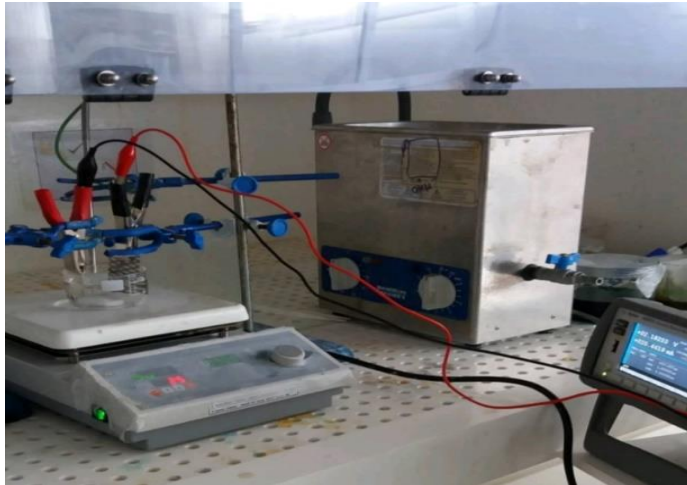
*Figure 3.2.* Plating equipment and test set-up

## 3.4. Roughness Measurements

Determination of surface suitability for specific work can be critical and this is provided by surface measurement. The surface measurement can be divided into more certain parts like as surface finish, surface shape, surface area roughness (Sa), surface profile roughness (Ra), surface texture and structural characterization.

The Zygo new view 5000 system 3D optical surface profiler was used with white light interferometer in measurements [55]. This device uses scanning white light interferometry technique during measurements. In addition, filtered white light and tungsten halogen lamp are used as a light source in this 3D optical surface profiler. The focusing can be performed manually or automatically and video monitor and on-screen display can be used as a part viewer in this device [55]. Moreover, it can be used transparent or opaque sample which has a specification with the reflectivity ranging from 4 to 100 %. The magnification can be set from 2.5x to 50x [55].

Three quality characteristics (levels) and three parameters were selected for experimental design. 3 levels mean $3^3 = 27$ total experiments. This is a full factorial

experimental design.  So, roughness values of these 27 coupons were determined. The selected parameters and their levels are given in the Table 3.2.

Table 3.2. *Selected parameters and levels for the experiments*

| Level | Duty Cycle (%) | Frequency (Hz) | Average Current Density (A/dm$^2$) | Peak Current (A/dm$^2$) |
|-------|---------------|----------------|-----------------------------------|------------------------|
| 1 | 10 | 10 | 0.5 | 5 |
| 2 | 50 | 40 | 1 | 2 |
| 3 | 75 | 80 | 1.5 | 1.125 |

## 3.5. S11 Measurements

An empirical test setup was set to measure the return loss (S11) according to the reference coupon which was coated with gold. An s-parameter vector network analyzer (8719ES S-parameter Vector Network Analyzer, 50 MHz to 13.5 GHz) was used to measure the scattering parameter from the test setup. The image of this setup is shown in Figure 3.3. This scattering parameter measurement setup belongs to a wr90 type of waveguide [54].
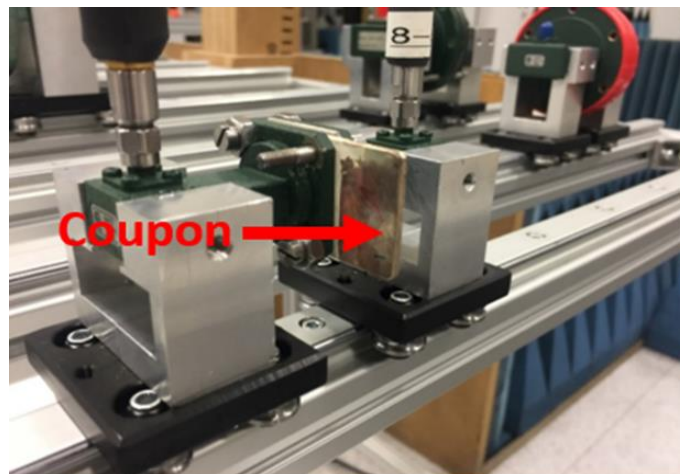


*Figure 3.3.* Image of set-up used to measure s-parameter

S11 setup was installed to measure a waveguide working at 10 GHz and 20 GHz. The inputs of the test coupons have the same interface with the input of the waveguide used in this device. Therefore, measurements were taken by placing coupons as waveguides in this experimental setup. In order to take the measurements, coupons were connected to the test setup as shown in Figure 3.3 and measurements were taken. After all coupons were measured, the S11 graphics were plotted with respect to the frequency. The S11 sequence between coupons was not changed regardless of the reference taken. The S11 graphs were plotted relative to a reference gold plate. Scattering parameters are complex because both the magnitude and the input signal phase can be altered by the system. The changes of S-parameters can be observed when there is a change in network, frequency, load impedance and source impedance. S11 parameter was measured according to schematic work in Figure 3.4. S11 is the reflection of the signal that was sent from port 1. The scattering parameter can be calculated by the ratio of two waves b1/a1 [56].
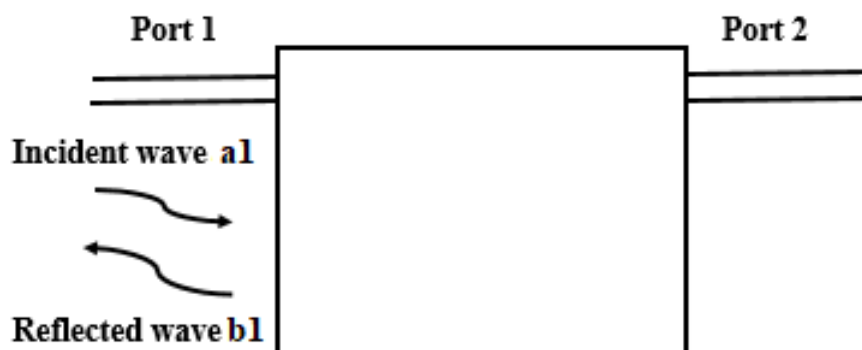


*Figure 3.4.* Schematic diagram for S11 parameter measurement

## 3.6. Surface Resistance Measurements

Surface resistances were measured using DT-5302 Miliohmmeter. ASTM Standard D257 was used as the measurement method. The resistance was measured in

Ohm/Square Meter. The flat surface of coupon was pressed with two probes of the Miliohmmeter on the coated surface for surface resistance measurements.

## 3.7. X-Ray Diffraction Measurements

In this work, Rigaku D/Max 2200/PC model X-Ray Diffractometer was used to take X-Ray diffraction patterns of samples by FT (counts) scanning. In the X-Ray diffractometer, generator settings were 40 kV and 40 mA and Cu Kα radiation at a wavelength of 0.154183 nm was used to obtain the X-Ray diffraction patterns. In addition, 2θ range from 10° to 90° were selected with the increments of 0.02° for taking X-Ray diffraction data of samples. The grain sizes were determined by calculating the peak widths according to the X-Ray diffraction patterns. The Scherrer equation was used to determine the grain size. In this equation, grain sizes are dependent on the full width at half-maximum (FWHM) value and the applied Scherrer constant. The peaks came from different silver orientations and phases. The FWHM method was used for calculating intensities of the peaks. The selection of Scherrer constant was not effective for the comparison of average grain size because the same Scherrer constant was used for each coupon to compare the grain sizes. The Scherrer equation is shown in Equation 16.

$$Dp = \frac{k\lambda}{\beta \cos \theta} \qquad (16)$$

$Dp$ =Average crystallite size (nm)

$k$ =Scherrer constant. It varies from 0.68 to 2.08. k = 0.94 for spherical crystallites with cubic symmetry

$\lambda$ =X-Ray wavelength.

$\beta$=FWHM (Full Width at Half Maximum) of XRD peak.

$\theta$ =XRD peak position, one half of 2θ

The β value is FWHM intensity of the peak. This value was calculated using *origin software*. The average crystallite size (nm) of the silver peaks at different orientations were calculated.

## 3.8. Microstructural Analysis

SEM analyzes were performed and high-resolution microstructure images were obtained using Nova NanoSEM. Energy distribution spectroscopy (EDS) analysis was performed by utilizing the EDS system in SEM. In this way, elemental analyses were made along the thicknesses of the coatings. In the selected samples, line scan analyses were performed using 2500x magnified images along the interface between the coating and the base material. The data was used to perform diffusion analysis. Coupons were cut and embedded in a bakalite material in order to determine elemental ratio with EDS line analysis from the vertical cross-sectional area. The Figure 3.5 shows coupons embedded in the bakalite. The variations of elemental data in the silver composition of a certain line in the cross-sectional area of the coupons were detected in this EDS analysis.



*Figure 3.5.* Prepared coupons for EDS line analysis

In addition to the samples shown in Figure 3.5, the coupons given in Figure 3.1 were used in SEM. The samples were cleaned and polished in order to get sharp images. The sizes of those samples were not reduced because samples fit to the sample holder. Conductive tape was used to ensure the conductivity between the samples and the bottom of the sample for samples shown in Figure 3.5. Image analysis was performed by using *ImageJ* program of SEM image [58]. High resolution images were taken from the surfaces of samples by scanning electron microscopy. The valley views that

come from pulse plating conditions in microstructure were calculated with using the *ImageJ* program by thresholding dark region of the SEM images. A strong contrast difference between the valleys and the rest of the SEM image was settled with *ImageJ* on the SEM images of coupons.

# CHAPTER 4


## RESULTS AND DISCUSSIONS


## 4.1. Effects of Pulse Electrodeposition Parameters on Surface Roughness

The duty cycle levels were selected as 10%, 50%, 75%; the frequency levels were selected as 10 Hz, 40 Hz, 80 Hz and the average current density levels were selected as 0.5 A/dm$^2$, 1 A/dm$^2$, 1.5 A/dm$^2$ in this study. In order to observe the effects of three parameters on the surface roughness, 27 experiments were performed. One more experiment was done to compare the differences between direct current coating and pulse current coatings. This is shown as the 28th experiment in Table 4.1. The surface roughness of 28 copper samples was measured before plating. The arithmetic average of the roughness profile taken from 27 samples was calculated as approximately as 0.270 μm. Differences of Ra values were insignificant because p value of roughness measurements was calculated as 0.923. Coupons were coated under 27 different conditions. The experimental conditions and the roughness values that were measured according to the selected parameters are shown in Table 4.1.

Table 4.1. *Experimental conditions and the roughness values*

| No. | Duty Cycle (%) | Frequency (Hz) | Average Current Density (A/dm²) | Peak Current (A/dm²) | Ra Roughness (μm) |
|---|---|---|---|---|---|
| 1 | 10 | 10 | 0.5 | 5 | 0.278 |
| 2 | 10 | 40 | 1 | 10 | 0.261 |
| 3 | 10 | 40 | 0.5 | 5 | 0.285 |
| 4 | 10 | 40 | 1.5 | 15 | 0.255 |
| 5 | 10 | 80 | 0.5 | 5 | 0.297 |
| 6 | 10 | 80 | 1 | 10 | 0.275 |
| 7 | 10 | 10 | 1 | 10 | 0.256 |
| 8 | 50 | 40 | 0.5 | 1 | 0.234 |
| 9 | 10 | 80 | 1.5 | 15 | 0.295 |
| 10 | 50 | 40 | 1 | 2 | 0.213 |
| 11 | 50 | 40 | 1.5 | 3 | 0.196 |
| 12 | 50 | 10 | 0.5 | 1 | 0.229 |
| 13 | 50 | 80 | 0.5 | 1 | 0.256 |
| 14 | 75 | 40 | 0.5 | 0.67 | 0.197 |
| 15 | 10 | 10 | 1.5 | 15 | 0.220 |
| 16 | 50 | 10 | 1 | 2 | 0.201 |
| 17 | 50 | 80 | 1 | 2 | 0.240 |
| 18 | 75 | 80 | 0.5 | 0.67 | 0.222 |
| 19 | 50 | 80 | 1.5 | 3 | 0.239 |
| 20 | 75 | 10 | 0.5 | 0.67 | 0.191 |
| 21 | 50 | 10 | 1.5 | 3 | 0.188 |
| 22 | 75 | 40 | 1 | 1.33 | 0.159 |
| 23 | 75 | 10 | 1 | 1.33 | 0.155 |
| 24 | 75 | 80 | 1 | 1.33 | 0.164 |
| 25 | 75 | 40 | 1.5 | 2 | 0.120 |
| 26 | 75 | 80 | 1.5 | 2 | 0.138 |
| 27 | 75 | 10 | 1.5 | 2 | 0.115 |
| 28 | 100 | - | 1.5 | - | 0.245 |

About 37.72% difference is present between the minimum and maximum of roughness values of selected parameters. Also, the surface roughness of silver coated sample by direct current of 1.5 A/dm² was measured as 0.245 μm before experiments. Surface profiles of uncoated copper coupon and a pulse silver coated sample are shown in

Figure 4.1. As can be seen in Figure 4.1, pulse silver coating caused an improvement in the surface profile. The pulse silver plating at 75% duty cycle, 10 Hz frequency and 1.5 A/dm$^2$ average current density was brought the surface roughness value to 0.115 µm.
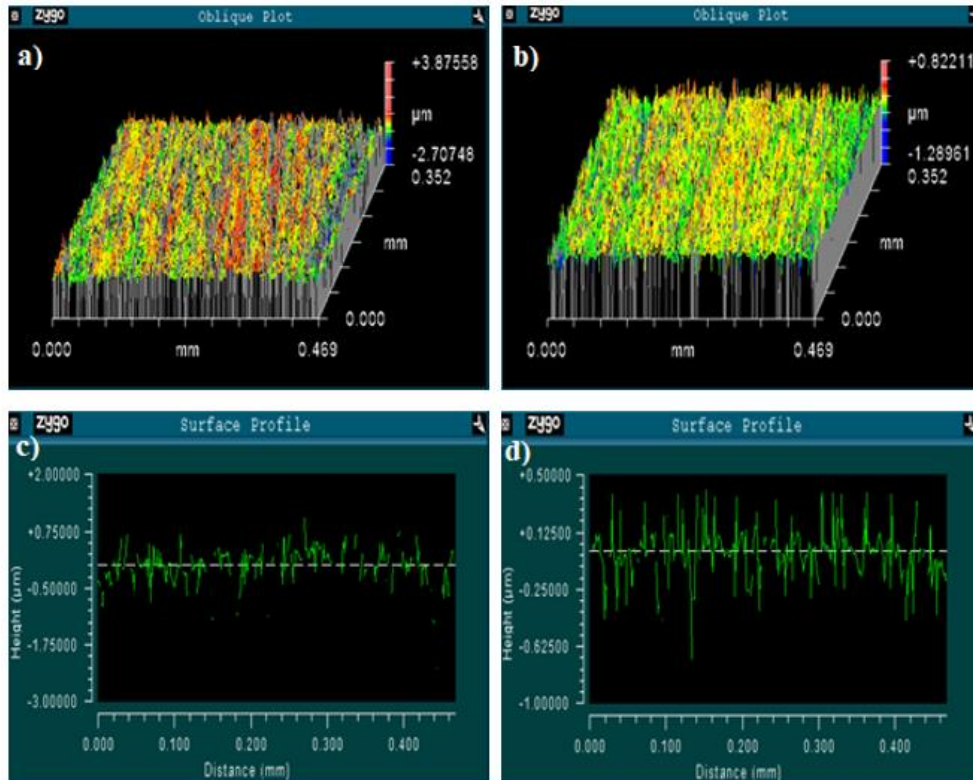


*Figure 4.1.* a) Oblique plot for a copper coupon; b) oblique plot for a silver coated coupon at Duty Cycle = 75 % Frequency= 10 Hz $I_a$= 1.5 A/dm$^2$; c) surface profile for a copper coupon; d) surface profile for a silver coated coupon at Duty Cycle = 75 % Frequency= 10 Hz $I_a$= 1.5 A/dm$^2$

The main effect graphics of duty cycle, frequency and average current density on surface roughness are shown in Figure 4.2 because the objective function was taken as roughness value in experimental design using Minitab program [12].
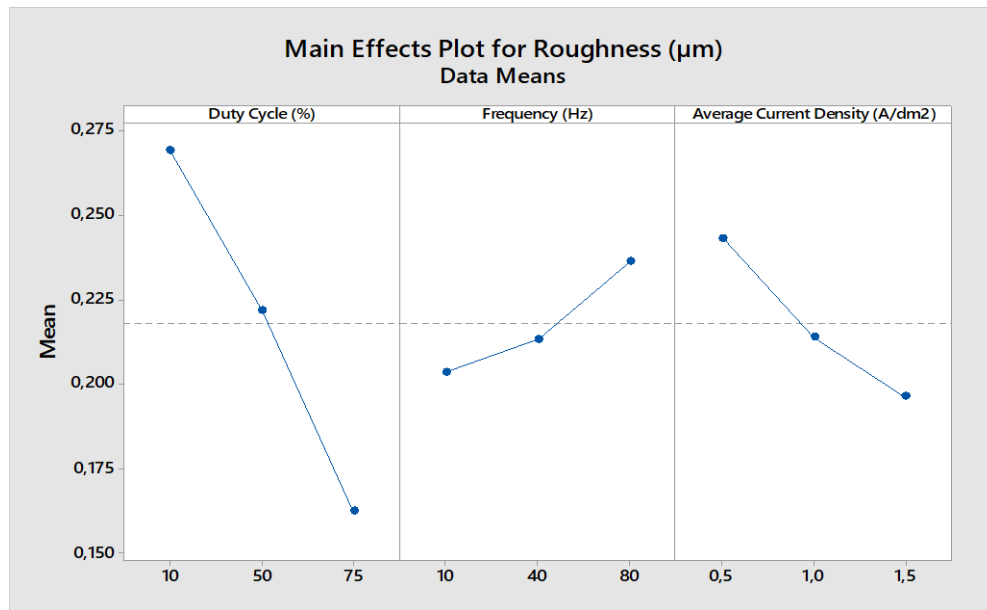
*Figure 4.2.* Main effects plot for roughness (µm)

As can be seen from Figure 4.2, when the duty cycle increases, frequency decreases and average current density increases; the surface roughness decreases within variation of parameters selected in this study. The main effects of the parameters on the surface roughness are very close to linear. The smoothest surface was reached at 75% duty cycle, 10 Hz frequency and 1.5 A/dm$^2$ average current density. However, since the relationship between variables was linear, it was necessary to measure the magnitude of the relationship between variables. As a result of multivariable experimental design, other variables affecting the dependent variable were considered as fixed and calculation was done according to this approach. How these variables affect the dependent variable was determined by regression analysis. The results of regression analysis are given in Appendix A. In the regression analysis, R$^2$ (Coefficient of Determination) was 91%. According to these results, the experiments can be repeated in terms of roughness value and can be called as statistically reliable. However, in order to understand how interaction affects the relationship between factors and response, their relationship should be evaluated graphically. The relation

graphs of frequency, duty cycle and average current density on roughness are shown in Figure 4.3.
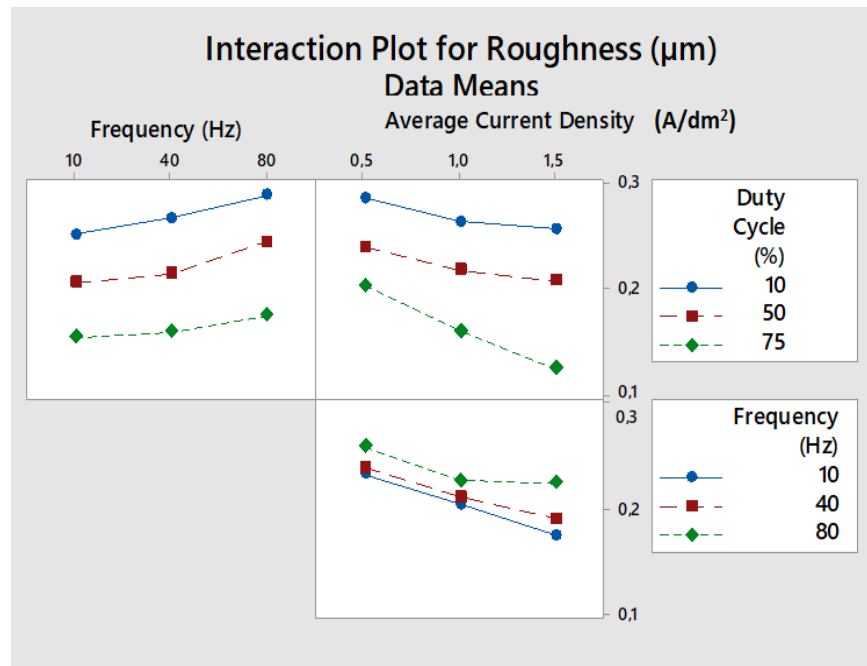


*Figure 4.3.* Interaction plot for roughness (µm)

When the duty cycle increases from 10% to 75%; the surface roughness decreases. When indicating the frequency graphs for all three levels, the surface roughness increases when the frequency increases. Average current density and duty cycle are proportional with surface roughness. Both increase the surface roughness value. Based on these two interactions, it can be stated that there is a negative effects on surface roughness between frequency and average current density. The interaction graphs confirm the main effect graphs on the roughness.

The surface roughness was better than the initial level after the pulse silver plating. However, the minimum surface roughness was achieved when the average current density was 1.5 A/dm$^2$ and duty cycle was 75%. When 100% duty cycle was obtained,

direct current was treated, and the surface roughness had a worse value. When the frequency increases, the duration period of current of coating increases. Nucleation occurs during on time period of the current. In addition to this, when the average current density increases, the nucleation rate increases. Although the increase in three parameters is thought to increase the nucleation rate; the optimum roughness value was obtained at the lowest frequency, highest duty cycle and highest average current density. This may be due to the increased nucleation rate with increasing the average current density, duty cycle and increased diffusion, grain growth when the frequency decreases. Diffusion is allowed over off time. For this reason, the pulse plating of silver was reduced the roughness of the outer layer plating with the high average current density, high duty cycle and low frequency. The level differences in the base material were further reduced after the coating. When the frequency increases, lower roughness value was observed. But decreasing frequency at a constant average current density and duty cycle yielded lower roughness value because the frequency was less effective on the roughness. As stated in Table 4.2, the duty cycle and average current density over the roughness value are more effective than frequency. Rank value explains this situation. The analysis of each control factor on the surface roughness was done by creating S/N response table using *minitab* program according to the results of the experiment S/N are logarithmic mean value of ratios. The most effective factors on surface roughness were duty cycle, average current density and frequency, respectively. The best value on roughness results of any parameter was found according to the largest S/N ratio obtained in all levels of that parameter. The delta value in Table 4.2 is the maximum and minimum differences of the respective variable over the surface roughness.

Table 4.2. *Response table for roughness value*

| Parameters | Duty Cycle (%) | Frequency (Hz) | Average Current Density (A/dm$^2$) |
|---|---|---|---|
| **Signal to Noise (S/N) Ratios for level 1** | 0.2691 | 0.2037 | 0.2432 |
| **Signal to Noise (S/N) Ratios for level 2** | 0.2218 | 0.2133 | 0.2138 |
| **Signal to Noise (S/N) Ratios for level 3** | 0.1623 | 0.2362 | 0.1962 |
| **Delta** | 0.1068 | 0.0326 | 0.0470 |
| **Rank** | **1** | **3** | **2** |

## 4.2. Effects of Pulse Electrodeposition Parameters on Scattering Parameter (S11)

A scattering parameter measuring device was installed for samples in Table 4.1. Seven graphs were drawn in the 12-18 GHz range with the s-parameter vector network analyzer according to a gold plate reference. S11 graph was plotted for 27 identified samples. However, comparative interpretation could be made for 7 of them that did not overlap each other along the frequency band and followed the same sequence continuously. The reason is that the antenna performance of the coupons other than these 7 coupons varies along the frequency band. At some frequencies, some coupons do not show the same tendency across the frequency band. To ensure the tendency of these seven coupons and the accuracy of the test measurement, S11 was plotted three times for seven coupons. Since the same sequence was generated in all three times, the S11 comparisons were evaluated using these seven parameters. Any material could be taken instead of reference gold. The return loss value may change when the material is changed. But the return loss order would not change between coupons. For this reason, return loss was not a definite value in these S11 measurements but it was only

used for performance comparison according to the selected reference. Therefore, the return loss versus frequency graphs for seven different coupons are shown in Figure 4.4.
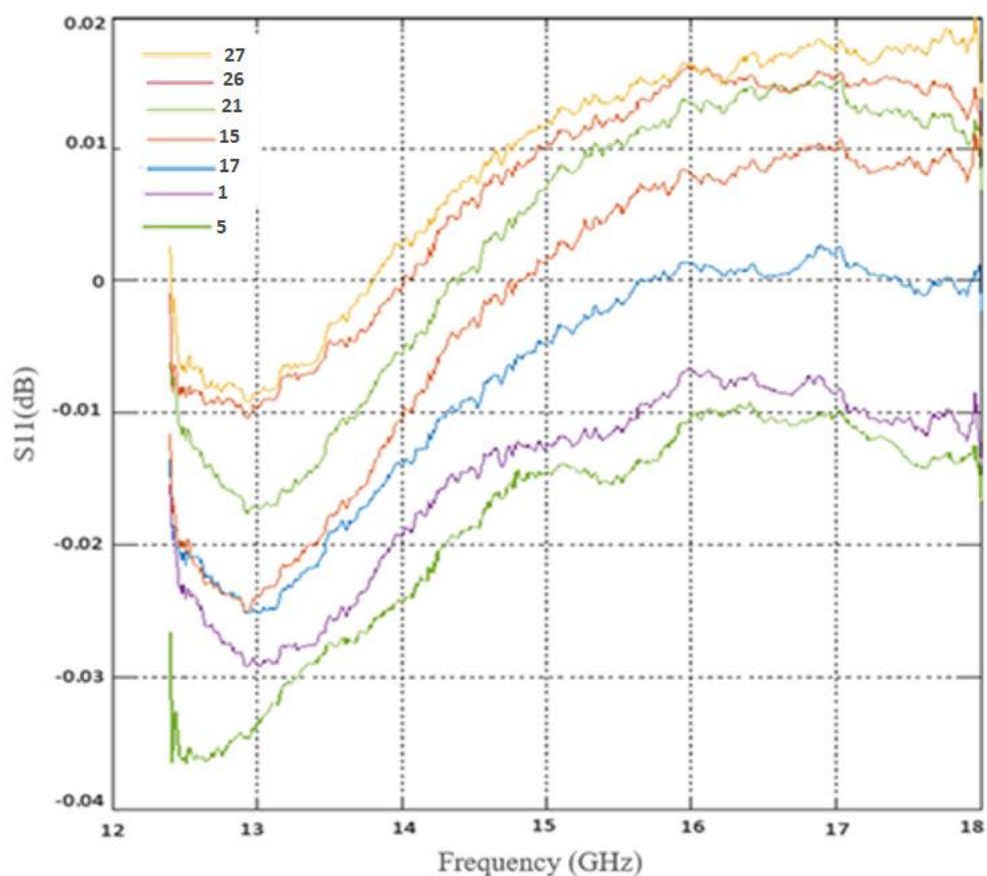


*Figure 4.4.* Return loss for different pulse parameters

The return loss differences between coupons are very low as shown in Figure 4.4. It can be thought that this is not enough to make comparisons. But, the most important point is that the order between coupons does not change during the 12-18 GHz frequency band. For example, the coupon with the highest loss has never crossed the foregoing coupon [57]. The top coupon has never changed its ranking. Therefore, this

sequence remained constant along the frequency band. The same measurement was repeated three times to ensure the reliability of the measurements. There was no change in rankings. Thus, the coating which has the least return loss have better electrical performance when conductive surface a waveguide is coated. In addition, the return loss will be more pronounced and more important when the working frequency of waveguides increases. These return losses will be very important in the Terahertz (THz) frequencies likewise very sensitive detection and imaging. Since the measurements are made at the coupon level, the return losses are very low due to the dispersion of the current on the surface of the material. However, this return loss will increase in the real complex and long waveguides. Because, there are faults caused by the coatings along the waveguide, the distribution of the current on the coated surface will change. Table 4.3 shows parameters and measured roughness values of seven samples for which scattering parameters (S11) were plotted in Figure 4.4.

Table 4.3. *Pulse silver plating parameters and roughness results*

| No. | Duty Cycle (%) | Frequency (Hz) | Average Current Density(A/dm$^2$) | The roughness (Ra) values (μm) |
|-----|------|------|------|------|
| 27 | 75 | 10 | 1.5 | 0.115 |
| 26 | 75 | 80 | 1.5 | 0.138 |
| 21 | 50 | 10 | 1.5 | 0.188 |
| 15 | 10 | 10 | 1.5 | 0.220 |
| 17 | 50 | 80 | 1 | 0.240 |
| 1 | 10 | 10 | 0.5 | 0.278 |
| 5 | 10 | 80 | 0.5 | 0.297 |

The roughness and the return loss (S11) values were directly proportional as can be seen from Table 4.3. The return loss on the rough surface increases slightly. It can be said that the return loss can change in relation to roughness in materials that have high conductivity. Reduction of frequency and increasing duty cycle may have an effect on conductivity. But the main effect comes from frequency and duty cycle and that is the roughness. In order to verify the effect of surface roughness on return loss, S11 measurements were taken again from coupons that were plated at three different pulse parameters. The S11 graphs drawn up as a result of these measurements are shown in Figure 4.5. The return losses in Figure 4.5 are much higher than the return losses in Figure 4.4. The reason for this difference is that S11 measurements presented in Figure 4.4 were taken on samples immediately after samples were removed from the bath. However, antitarnishing was applied to coupons after coating and the S11 measurements were taken a few days later in the case of results presented in Figure 4.5.
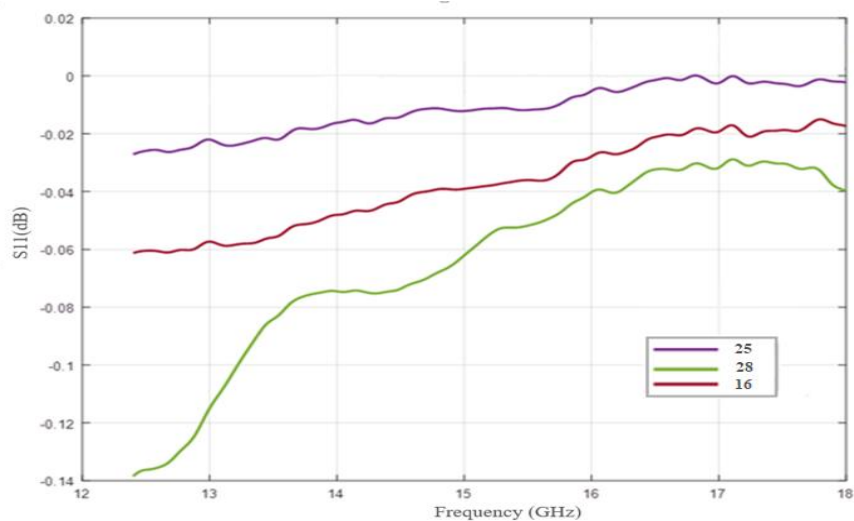


*Figure 4.5.* Return loss relative to the reference gold plate; no 25: 75 Duty Cycle (%) 40 Frequency (Hz) 1,5 Average Current Density (A/dm$^2$); no 28: 100 Duty Cycle (%) no 16: 50 Duty Cycle (%) 10 Frequency (Hz) 1 Average Current Density (A/dm$^2$)

When the duty cycle and the average current density increased, the return loss decreased as can be seen from Figure 4.5. The return losses were much more than the others for coating that was made by direct current i.e. at 100% duty cycle. The second measurement results in Figure 4.5 also confirmed that the relationship of return losses which is proportional to the surface roughness.

Another important point is that the effect of return loss changes very little because, factors affecting the conductivity rather than the roughness is more important in return loss measurements. Roughness did not change the conductivity much since conductivity for a silver coating, which is already a very well conductor, will always be satisfactory up to 30-40 GHz. Therefore, this effect will be seen more clearly in less conductive materials. As can be seen from Figure 4.4, the return loss and roughness at very high and very low frequencies are not changed too much. But, when the duty cycle fell from 75% to 10%, the roughness nearly doubled when the frequency and average current density were constant. The roughness was almost the same when the frequency increased from 10 Hz to 80 Hz at 10% duty cycle and 0.5 A/dm$^2$ average current density. However, this situation was observed more clearly in return loss graphs than roughness results. Changing the plating material's internal structure as a result of pulse parameters may be the reason for this situation. So, grain structure may be more affective in changing of the roughness by changing the frequency.

Finally, in order to verify the return loss differences between uncoated copper coupon and silver-plated coupons, S11 comparisons were made between the copper and two silver-plated samples which were coated by direct and pulse currents. Silver coated coupons had lower return losses than copper coupon as can be seen from Figure 4.6. This is because silver has higher conductivity than the copper.
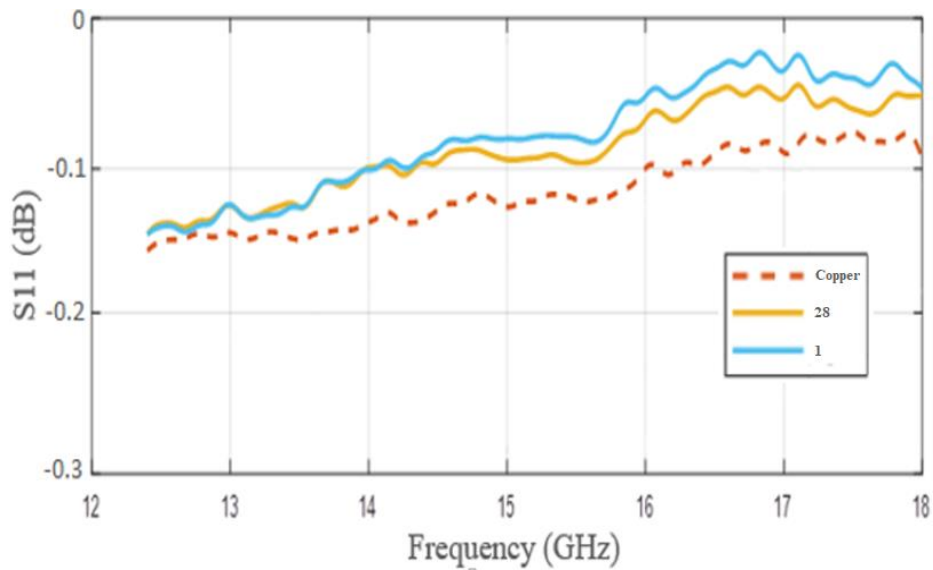
*Figure 4.6.* Return loss between a copper coupon; no 28: a silver plated sample which was coated by direct current; no 1: a silver plated sample which was coated by pulse current

## 4.3. Microstructural Examination

Microstructures of coatings were analyzed to reveal effects of pulsed silver-plating parameters on the morphology of surfaces. SEM images were taken at the same magnification. It is known that pulse electrodeposition causes dendritic structure and pyramidal and globular grain growth [41, 42]. The SEM images shown in Figure 4.7 were taken from two samples which were coated under two different conditions. The aim is to observe effects on the microstructure when the duty cycle, frequency and average current density increase at the same time.

When nucleation sites increase, grain sizes of the silver coating decrease as shown in Figure 4.7. When the average current density increases, in direct current coatings as well, the nucleation rate increases. However, the frequency and duty cycle are as effective as the current density in coatings made with pulsed current as shown in microstructure image in Figure 4.7. It was examined that when all of the average current density, frequency and duty cycle were increased, more nucleation occurred

while is being plated. Therefore, these three parameters should be considered together when evaluating the nucleation rate.
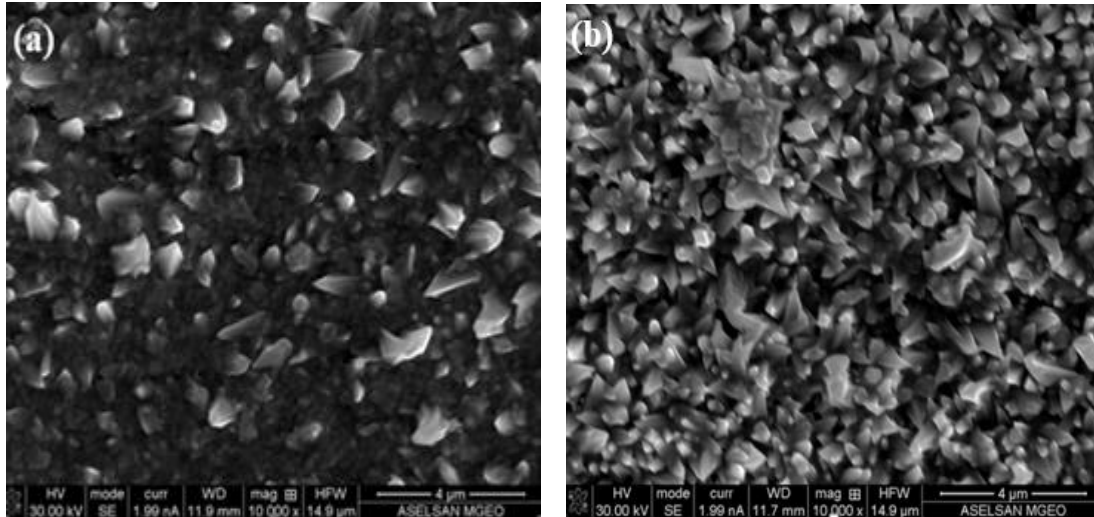


*Figure 4.7.* Grain structures of coatings at a) 50 Duty Cycle (%) 10 Frequency (Hz) 1 Average Current Density (A/dm$^2$) and b) 75 Duty Cycle (%) 40 Frequency (Hz) 1.5 Average Current Density (A/dm$^2$)

Pulse period, $t_{on}$ and $t_{off}$ are effective on the grain growth because nucleation takes shape throughout the on time and growth of grains proceeds throughout the off time. To understand the influence of frequency on microstructure or grain structure, charging and discharging of the double layer must be evaluated. There is not enough time for this double layer to load or unload at high frequencies. After observing the effect of the increment of these three parameters on the microstructure, the six samples which were pulse coated under different conditions were selected to observe the effect of each of the parameter on the microstructure. Initially, the effect of average current density on microstructure was observed at a fixed frequency and duty cycle. SEM images of two samples which were plated at 80 Hz frequency, 75 Duty Cycle (%) and 1.5 A/dm$^2$ average current density and at 75% duty cycle, 80 Hz frequency, 0.5 A/dm$^2$ average current density are shown in Figure 4.8. There is a pyramidal growth for both cases in Figure 4.8. The increase in average current density caused more congested

and finer grained morphology. If the coating had not been applied using pulsed current, the orientation would be less and probably a hollower structure would be obtained. The high frequency and duty cycle have been effective in making the structure more uniform at 1.5 A/dm$^2$. This change can also be caused by an increase in overpotential. This theory is explained by a basic electrodeposition theory. The cathode current density increases the cathode overpotential. This reduces the critical radius of nucleation [41, 44]. Because the nucleation rate increases, a denser and refined structure is obtained. The structure which is given in Figure 4.7 at 1.5 A/dm$^2$ supports this theory.
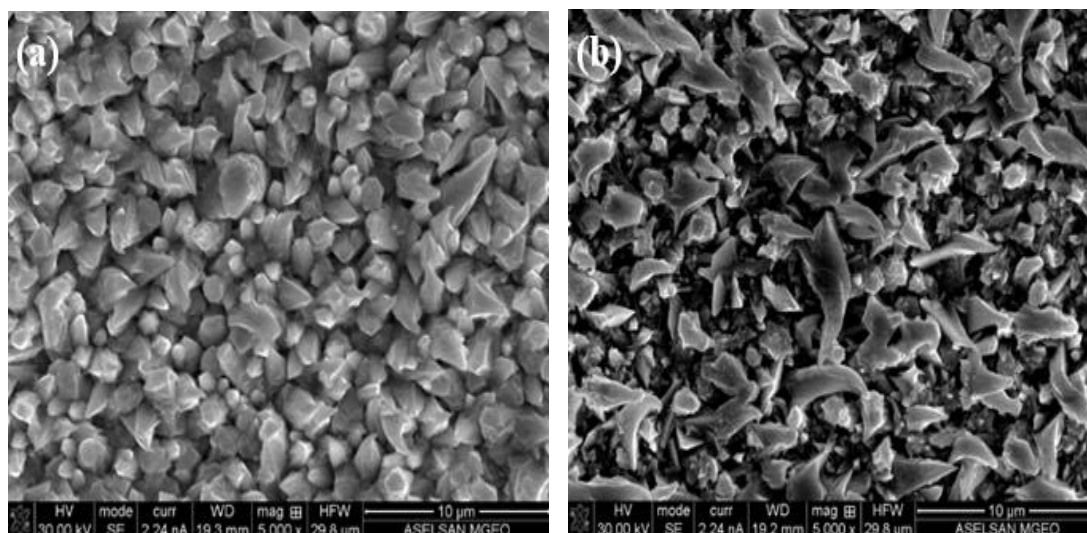


*Figure 4.8.* Grain structures of coatings at a) 75 Duty Cycle (%) 80 Frequency (Hz) 1.5 Average Current Density (A/dm$^2$) and b) 75 Duty Cycle (%) 80 Frequency (Hz) 0.5 Average Current Density (A/dm$^2$)

Figure 4.9 shows the effect of frequency at 75% duty cycle and at 0.5 A/dm$^2$. When the frequency was increased, the structure became smaller and homogeneous. Structural morphology did not change.

As a result of the above experimental observations, the frequency is also effective on the microstructure. When pulse frequency increases, the electric field decreases so the

time of the movement of ions and the pulse width decreases. This change triggers crystal nucleation. When the frequency increases at fixed duty cycle, the ratio of on time to off time does not change. But the time period between on time and off time are reduced. In addition, when the frequency increases, this decreases the concentration overpotential in some cases. In short, if the frequency increases more compact, small and homogeneous microstructures occur.
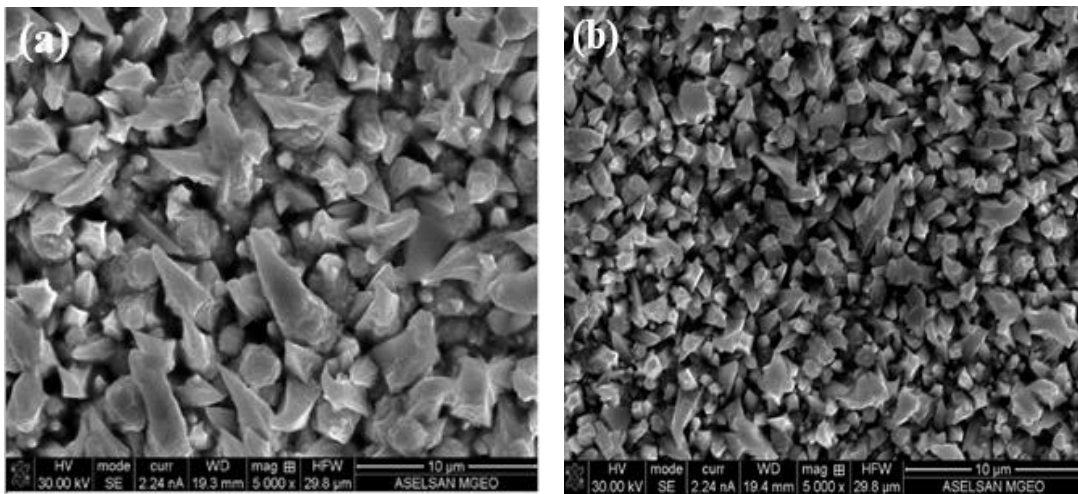


*Figure 4.9.* Grain structures of coatings at a) 75 Duty Cycle (%) 10 Frequency (Hz) 0.5 Average Current Density (A/dm$^2$) and b) 75 Duty Cycle (%) 40 Frequency (Hz) 0.5 Average Current Density (A/dm$^2$)

The effects of the change of duty cycle and average current density were observed at the same time in Figure 4.10. Figure 4.7-4.9 confirm the observations in Figure 4.10. When the duty cycle decreased, the grain structure grew. More homogenous structures were observed at high duty cycle and average current density. Orientations were reduced at low duty cycle and low average current density. However, when duty cycle and average current density increased, homogeneous grain structure was obtained.
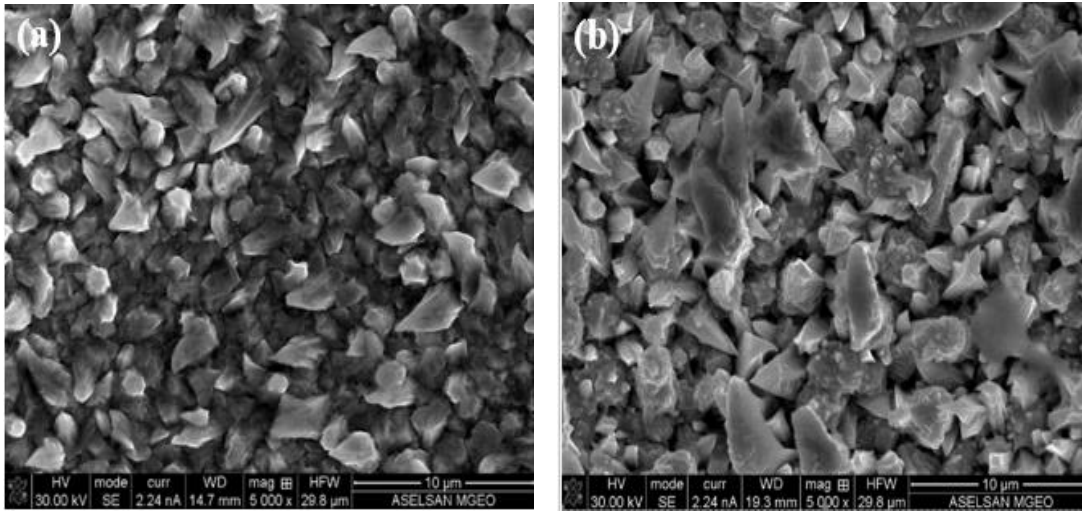
*Figure 4.10.* Grain structures of coatings at a) 75 Duty Cycle (%) 10 Frequency (Hz) 1.5 Average Current Density (A/dm$^2$) and b) 10 Duty Cycle (%) 10 Frequency (Hz) 1 Average Current Density (A/dm$^2$)

As can be seen from morphologies in SEM images, microstructures show pyramidal growths. However, in some pulse electrodeposition conditions, more black regions were seen. The excess of these regions led to the formation of similar structures to have valleys in morphology. The *ImageJ* software was used to determine the valleys in the morphology of the pulsed silver coatings from a SEM images (e.g., Figure 4.11a). It can also be used to make the thresholding. The ratio of hills to whole structure was calculated by *ImageJ* 'Particle Analyze' feature. Figures 4.11b and 4.11c respectively show binary and thresholder images. The numbers reported in the inner part of Figure 4.11d are the sequential index of the valleys. The ratio of the red area to the total area was calculated as the fraction of dark black regions according to Equation 17 [58].

$$\phi = \frac{\sum_{i=1}^{n}(A_i)}{A} \qquad (17)$$

Where $A_i$ and A are the area of each i$^{th}$ calculated black region and all area of the image respectively. The percentage black regions calculated from the SEM images by the *ImageJ* program are shown in Appendix B.

60
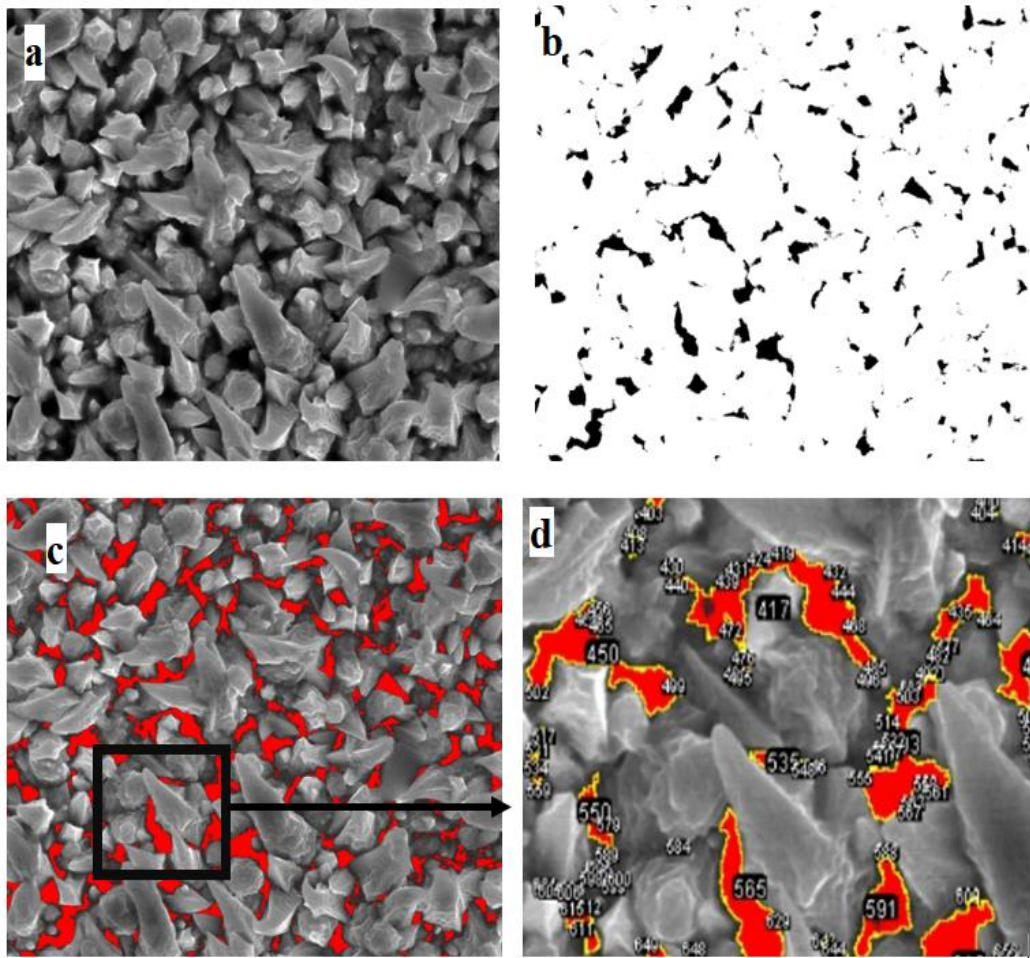
*Figure 4.11.* (a) SEM image of a pulse silver plating; (b) the corresponding binary converted black and white image with white index and black regions; (c) black area pointed out in red after image thresholding; (d) a zoomed-in view of the identified the hills

Duty cycle, frequency and average current density have affected the pyramidal growth and valleys in the morphology. As can be seen in Table 4.4, increasing frequency, duty cycle and average current density decreases valleys in the morphology.

Table 4.4. *Dark regions in SEM images ratios for different pulse parameters*

| No. | % Dark Regions in SEM Images | Duty Cycle (%) | Frequency (Hz) | Average Current Density (A/dm$^2$) | Peak Current Density (A/dm$^2$) |
|---|---|---|---|---|---|
| 26 | 3.9 | 75 | 80 | 1.5 | 2 |
| 24 | 4.1 | 75 | 80 | 1 | 1.33 |
| 18 | 4.4 | 75 | 80 | 0.5 | 0.66 |
| 27 | 5.8 | 75 | 10 | 1.5 | 2 |
| 20 | 6.2 | 75 | 10 | 0.5 | 0.66 |
| 14 | 6.3 | 75 | 40 | 0.5 | 0.66 |
| 16 | 7.5 | 50 | 10 | 1 | 2 |

## 4.4. X-Ray Diffraction (XRD) Analysis

XRD diagrams of pulse silver coatings which were prepared at different pulse parameters are shown in Figure 4.12.
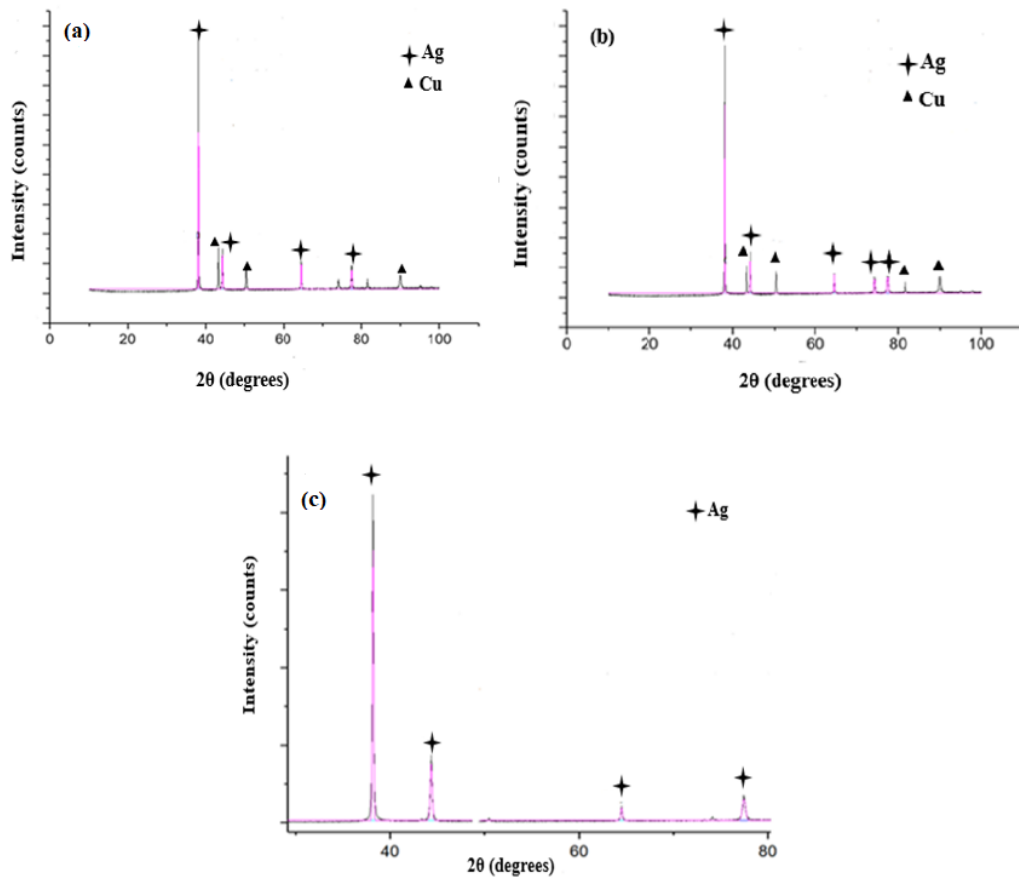
Figure 4.12. X-Ray Diffraction (XRD) patterns of pulse silver coating at (a) Duty Cycle = 50 % Frequency= 10 Hz Ia= 1 A/dm$^2$, (b) Duty Cycle = 75 % Frequency= 40 Hz Ia= 0.5 A/dm$^2$ (c) Duty Cycle = 75 % Frequency= 10 Hz Ia= 1.5 A/dm$^2$

The XRD diagrams of samples which were plated by using seven different pulse parameters are indicated in Appendix C. As being stated in Appendix C, only the four primaries of all five reflection lines for Ag have been noted. These primary reflection lines are (111), (200), (220) and (311).  Diffraction lines of (222) is the second-order diffraction of (111) plane. The strongest peak of randomly oriented polycrystalline silver was obtained from (111) plane. Silver has face-centered cubic (FCC) lattice. Atomic density of (111) plane is higher than atomic density of other planes for silver. This means; the surface energy of plane (111) was lower than the surface energy of other planes. In XRD diagrams, copper peaks were detected in some conditions. This can be taken from the base copper material. As can be seen from silver XRD patterns,

the intensity of the peaks and the reflection angles are in accord with the Bragg law changes. This Bragg's law is given in Equation 18.

$$n\lambda = 2d_{hkl}\sin\theta \qquad (18)$$

Where n is the order of reflection, $\lambda$ is the X-Ray wavelength, $d_{hkl}$ is the interplanar separation for a plane having indices h, k and l and $\theta$ the angle of diffraction for constructive interference. The $d_{hkl}$ is proportional to the lattice parameter. Therefore, it can be stated that $d_{hkl}$ decreases when $\theta$ increases. From this point of view, the change of the Bragg angle can also affect the crystal size. Scherrer's Formula in Equation 16 [59] explains this situation. The crystallite sizes of silver which is plated using different pulse parameters are shown in Table 4.5. The calculation of the Ag crystallite size (nm) for pulse silver coatings that were made in each condition are shown in Appendix C.

Table 4.5. *Ag crystallite size (nm) at different pulse conditions*

| No. | Ag crystallite size (nm) | Duty Cycle (%) | Frequency (Hz) | Average Current Density (A/dm²) | Peak Current Density (A/dm²) |
|-----|--------------------------|----------------|----------------|---------------------------------|-------------------------------|
| 26 | 40.92 | 75 | 80 | 1.5 | 2 |
| 24 | 42.13 | 75 | 80 | 1 | 1.33 |
| 18 | 48.64 | 75 | 80 | 0.5 | 0.66 |
| 27 | 48.7 | 75 | 10 | 1.5 | 2 |
| 20 | 59.12 | 75 | 10 | 0.5 | 0.66 |
| 14 | 59.09 | 75 | 40 | 0.5 | 0.66 |
| 16 | 63.09 | 50 | 10 | 1 | 2 |
| 7 | 70.74 | 10 | 10 | 1 | 10 |

As it can be seen from the results, the grain size of the silver atoms decreases when frequency and duty cycle increases. The pulse deposition rate is related to the on time and off time periods. In addition, the grain size is directly related to on time and off time. Increasing the on time causes more nucleation in the plating. The period decreases as the frequency increases so the time between on time and off time decreases. When duty cycle increases, on time increases and the nucleation rate increases as the duration of current application increases. Since high frequency and high duty cycle increase nucleation rate and decrease duration of the off time, smaller and homogeneous grain structure is formed.

However, increasing pulsed current density at constant peak current density and at fixed off time causes a decrease of the grain size. In this way, a short on time counteracts growth of grain and expands the nucleation rate. It has inverse relationships with the frequency. A longer period at low frequencies gives enough time for the charging and discharging of the double layer. Conversely, the double layer does not possess enough time for charging and releasing at high frequencies. Therefore, larger grain structure was obtained at low frequencies in this work. Grain refinement occurred at high frequencies. Figure 4.13 shows the frequency and duty cycle effects on the Ag crystallite size obtained by using different pulse parameters in Table 4.5. As shown in Figure 4.13, increasing frequency and duty cycle reduce the grain size.
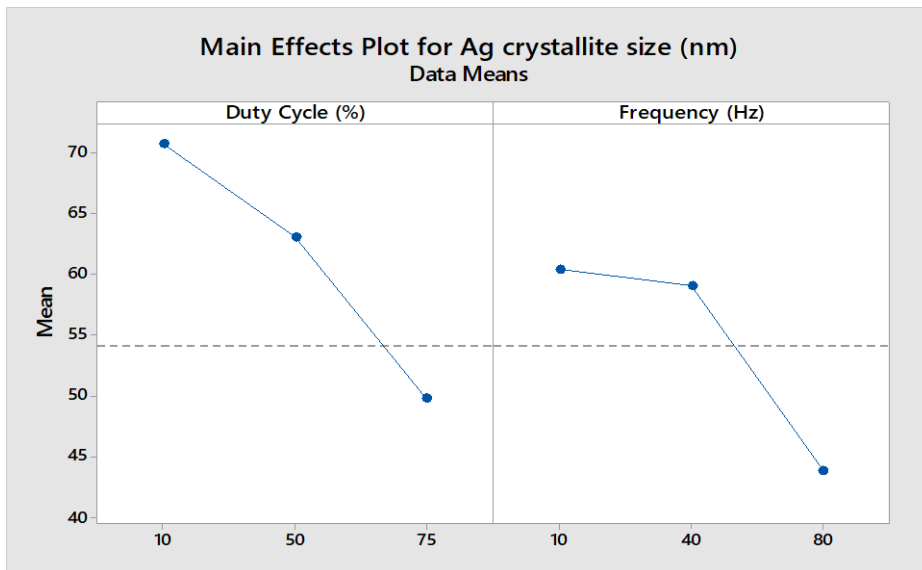
*Figure 4.13.* Main effects plot for Ag crystallite size (nm)

## 4.5. Energy-Dispersive Spectrometer (EDS) Line Analysis

Ion transport from solution to cathode occurs during electrolytic coatings. At the cathode, there is a diffusion of the metal to be coated by electron transfer into the base metal material. Under normal conditions, this diffusion is very difficult in an electroless environment, however it can be very fast due to kinetic factors with the presence of electrical current during coating [60]. In order to determine the proportion of these atoms and the extent to which they can diffuse in the silver plating in the vertical cross-sectional area, EDS line analysis was performed. The analysis was performed along a line between silver and copper perpendicular to the interface on the cross-sectional area of the sample as can be seen in Figure 4.14.

Magnification: x10.000 ——— 5µm
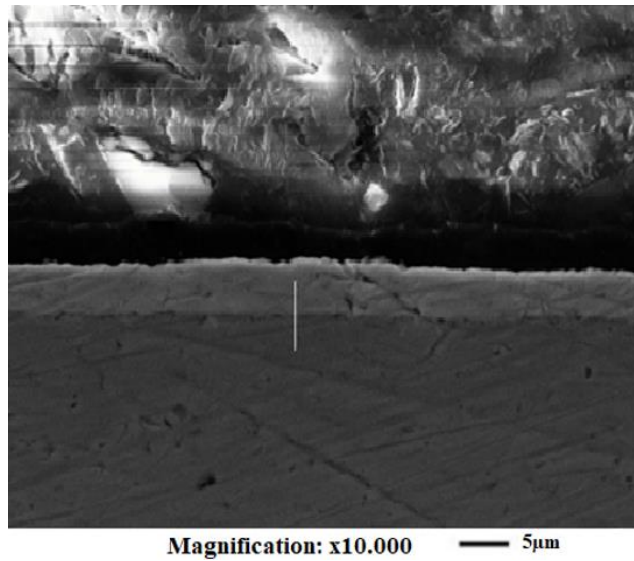
*Figure 4.14.* Cross-sectional SEM image of the diffusion area

This line was selected between the regions where transition from approximately 100 % Cu to 100% Ag atoms takes place. As a result of EDS analysis, total intensity amounts of atoms were obtained along the line. However, the highest intensity value has not changed after a certain distance. If this intensity was too high and didn't change, it can be said that there was no diffusion in that area. For example, in the copper region of Figure 4.15, the intensity of copper atoms was the greatest at the bottom of the line. If the calculated copper intensity along the line was divided to the highest intensity value of copper, the amount of change of copper atoms could be plotted with respect to the distance. EDS analysis was applied to a pulse-coated sample obtained at 50 Duty Cycle (%), 10 Frequency (Hz) and 1 Average current Density (A/dm$^2$) values. Ag% content versus distance graph was drawn as a result of EDS line analysis. This graph is shown in Figure 4.15.
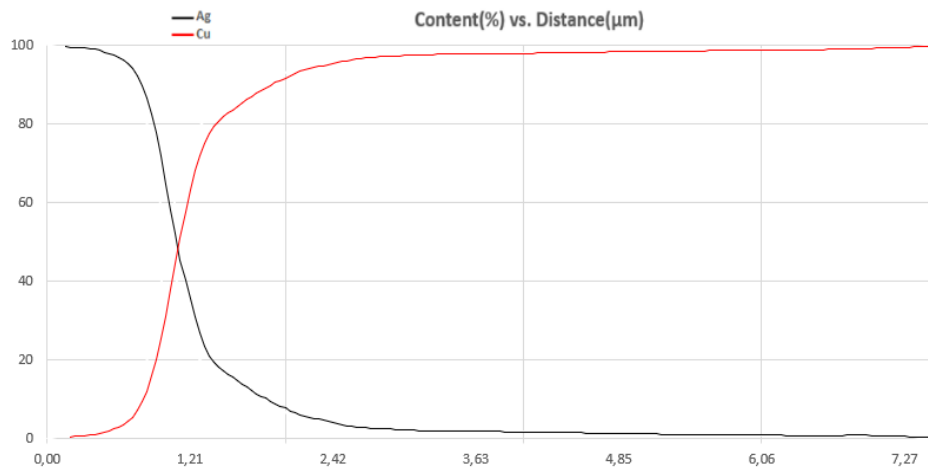
*Figure 4.15.* Percentages of Ag and Cu versus distance graph at 50 Duty Cycle (%), 10 Frequency (Hz) and 1 Average Current Density (A/dm$^2$)

As can be seen in Figure 4.15, the distance between the highest point where the silver ratio does not change and the lowest point where the silver ratio does not change was calculated as 0.88 μm. In fact, since the outermost surface contains a high-thickness silver layer, only the diffusion occurs at 0.88 microns. The effect of the changing pulse parameters on this silver diffusion region was calculated in Appendix D for four different parameters. At the same time using the graphics obtained in Appendix D, Diffusion Coefficients of Ag in Cu was obtained for four different cases. The calculated values are shown in Table 4.6.

Table 4.6. *Diffusion zone of silver change with different pulse parameters*

| No. | Diffusion Zone(μm) | Duty Cycle (%) | Frequency (Hz) | Average Current Density (A/dm²) | Peak Current Density (A/dm²) | Diffusion Coefficients of Ag in Cu (m²/s) |
|---|---|---|---|---|---|---|
| 26 | 0.61 | 75 | 80 | 0.5 | 0.66 | $1.41 \times 10^{-20}$ |
| 14 | 0.88 | 75 | 40 | 0.5 | 0.66 | $7.29 \times 10^{-20}$ |
| 16 | 0.98 | 50 | 10 | 1 | 2 | $1.56 \times 10^{-19}$ |
| 7 | 1.96 | 10 | 10 | 1 | 10 | $2.73 \times 10^{-18}$ |

The Diffusion Coefficients of Ag in Cu is $1.273 \times 10^{-28}$ m²/s at room temperature in an inert media [61]. However, the current generated by the electron transfer during coating increases the diffusion coefficient to ensure that the diffusion occurs in a certain range. When the current is removed from the environment, when the coating is completed, diffusion returns to its value in the no-current environment and diffusion becomes infeasible.

According to the results in Table 4.6, the most important parameter in this silver diffusion was the peak current density. Because when the peak current density was increased, the maximum current value has increased and the transport of Ag atoms by kinetic factors accelerated.

# CHAPTER 5

# CONCLUSION

The effect of pulse silver plating parameters on the surface roughness of the coating and the effect of pulse silver plating parameters on the scattering parameters or return loss (S11) which was used to determine the performance of microwave products (antennas and waveguides) were determined.

According to the results, it was found that decreasing the frequency, increasing the duty cycle and increasing the average current density reduce the surface roughness. It was interfered that the duty cycle was the most effective on roughness among the pulse coating parameters. Return loss (S11) was measured according to a reference gold-plated sheet on 7 out of 27 samples. The scattering parameter S11 was found to increase with the surface roughness. Therefore, return loss (S11) was decreased with the increase of duty cycle and average current density.

It was indicated that coatings made by the pulse current has less return loss compared to the direct current coating. After the roughness and scattering parameter measurements, SEM images were taken from 11 samples which were plated at different pulse parameters to analyze the microstructure of the silver coating and to understand the microstructural effects on surface roughness and return loss. After the examination of the SEM images, it was seen that the pulse plating causes the pyramidal structures. In addition, valley-like structures within the microstructure have changed with the change of pulse parameters.

X-Ray Diffraction (XRD) analysis was performed to determine grain sizes and elemental contents of coatings. According to X-Ray Diffraction (XRD) analysis, it was observed that the intensity of silver peaks and XRD peak positions changed with pulsed silver-plating parameter. Crystallite size calculations were performed using

XRD data. According to the results, it was understood that the Ag crystallite size varies inversely with frequency and duty cycle.

According to the results of elemental analysis from the result of EDS analysis, it was determined that the increase in duty cycle and frequency caused a negative effect on diffusion zone of Ag. It was found that the main effect on diffusion zone was caused by peak current density increased silver diffusion.

# REFERENCES

[1] The Editors of Encyclopaedia Britannica. Silver. *Encyclopædia Britannica.* February 07, 2019. [Cited: 04 03, 2019.] https://www.britannica.com/science/silver.

[2] Syafiuddin, A., Salmiati, Salim, M. R., Beng Hong Kueh, A., Hadibarata, T., & Nur, H. (2017). A Review of Silver Nanoparticles: Research Trends, Global Consumption, Synthesis, Properties, and Future Challenges. *Journal of the Chinese Chemical Society*, 64(7), 732–756. https://doi.org/10.1002/jccs.201700067

[3] Seshadri, S. K. (1990). pulse plating review. *Time*, *25*, 439–461.

[4] Balanis, C. A. (1989)*. Advanced Engineering Electromagnetics.* John Wiley & Son.

[5] Fong, A., Coackley, R., Dupre, J. J., Greer, S. J., Linkwitz, S., Page, J. R., … Sasaki, G. D. (2002). 12 - Measurements and Analysis. In W. M. Middleton & M. E. Van Valkenburg (Eds.), *Reference Data for Engineers (Ninth Edition)* (Ninth Edition, pp. 12–39).

[6] Zhang, P., Wyman, I., Hu, J., Lin, S., Zhong, Z., Tu, Y., … Wei, Y. (2017). Silver nanowires: Synthesis technologies, growth mechanism and multifunctional applications. *Materials Science and Engineering: B*, *223*, 1–23.

[7] Szeftel, J., Sandeau, N., & Khater, A. (2017). Study of the skin effect in superconducting materials. *Physics Letters A*, *381*(17), 1525–1528.

[8] Durney, L.J. (1984*). Electroplating Engineering Handbook. 4th ed*. London: Chapman & Hall.

[9] Osero, N. M. (1986). An overview of pulse plating. *Plat. Surf. Finish.*, Vol. 73, pp. 20–22.

[10] Chandrasekar, M. S., & Pushpavanam, M. (2008). Pulse and pulse reverse plating-Conceptual, advantages and applications. *Electrochimica Acta*, *53*(8), 3313–3322.

[11] Mehdizadeh, M. (2015). Chapter 8 - RF/microwave applicators and systems for joining and bonding of materials. In M. Mehdizadeh (Ed.), Microwave/RF Applicators and Probes (Second Edition) (Second Edition, pp. 269–300). https://doi.org/https://doi.org/10.1016/B978-0-323-32256-0.00008-7

[12] Antony, J. (2014). 7 - Fractional Factorial Designs. In J. Antony (Ed.), Design of Experiments for Engineers and Scientists (Second Edition) (Second Edition, pp. 87–112). https://doi.org/https://doi.org/10.1016/B978-0-08-099417-8.00007-9

[13] A. David Olver, P. J. Clarricoats (1994). *Microwave Horns and Feeds*. IEE Press, IEE Electromagnetic Waves Series 39

[14] G. M. Rebeiz, L. P. B. Katehi, W. Y. Ali-Ahmad, G. V. Eleftheriades and C. C. Ling, "Integrated horn antennas for millimeter-wave applications," in *IEEE Antennas and Propagation Magazine*, vol. 34, no. 1, pp. 7-16, Feb. 1992.

[15] Bernard, J., Marconi, T., Limited, C., Engi, A., Wimer, P. E. C., & Le, A. E. (1991). *United States Patent (19)*. (19), 3–8.

[16] T. S. Chu and R. A. Semplak, "Gain of electromagnetic horns," in *The Bell System Technical Journal*, vol. 44, no. 3, pp. 527-537, March 1965.

[17] A. P. King, "The Radiation Characteristics of Conical Horn Antennas," in *Proceedings of the IRE*, vol. 38, no. 3, pp. 249-251, March 1950.

[18] Daniels, D. J. (2009). Chapter 4 - Antennas. In H. M. Jol (Ed.), *Ground Penetrating Radar Theory and Applications* (pp. 99–139). https://doi.org/https://doi.org/10.1016/B978-0-444-53348-7.00004-1

[19] Francis, M. N., & Howard, F. R. (1936). The electrical conductivity of transition metals. *Proceedings of the Royal Society of London. Series A - Mathematical and Physical Sciences*, *153*(880), 699–717. https://doi.org/10.1098/rspa.1936.0031

[20] Issn, I. I., & Engineering, M. (2004). *DFM ( A ) - Aspects For A Horn Antenna Design Dr . Harri Eskelinen Mikko Tuunanen Raimo Suoranta Prof . Pertti Silventoinen*.

[21] H. A. Wheeler, "Formulas for the Skin Effect," in *Proceedings of the IRE*, vol. 30, no. 9, pp. 412-424, Sept. 1942.

[22] Mattis, D. C., & Bardeen, J. (1958). Theory of the Anomalous Skin Effect in Normal and Superconducting Metals. *Phys. Rev.*, *111*(2), 412–417.

[23] Pozer, D. (2005). *Microwave Engineering Third Edition*. John Wiley & Son

[24] Hewlett-Packard Application Note 154. (1972). S Parameter Design.

[25] J. B. Mohler and H. J. Sedusky, Nickel Plating, in Electroplating Chemical Publishing Co.: New York, 1951.

[26] J. L. Stojak, J. Fransaer and J. B. Talbot, Review of Electrocodeposition, in Advances in Electrochemical Science and Engineering Wiley-VCH Verlag GmbH, p. 193, 2001.

[27] Sato, N. (1998). Chapter 7 - Electrode Reactions. In N. Sato (Ed.), *Electrochemistry at Metal and Semiconductor Electrodes* (pp. 213–233). https://doi.org/https://doi.org/10.1016/B978-044482806-4/50007-6

[28] Scholz F. (2005) Thermodynamics of Electrochemical Reactions. In: Scholz F. (eds) Electroanalytical Methods. Springer, Berlin, Heidelberg

[29] Garrido, J. (2004). Thermodynamics of Electrochemical Systems. *The Journal of Physical Chemistry B*, *108*(47), 18336–18340. https://doi.org/10.1021/jp049264o

[30] Grimnes, S., & Martinsen, Ø. G. (2015). Chapter 7 - Electrodes. In S. Grimnes & Ø. G. Martinsen (Eds.), *Bioimpedance and Bioelectricity Basics (Third Edition)*(Third Edition, pp. 179–254). https://doi.org/https://doi.org/10.1016/B978-0-12-411470-8.00007-6

[31] Ciobanu, M., Wilburn, J. P., Krim, M. L., & Cliffel, D. E. (2007). 1 - Fundamentals. In C. G. Zoski (Ed.), *Handbook of Electrochemistry* (pp. 3–29).

[32] F. A. Lowenheim, *Modern Electroplating*, in *Nickel*, H. Brown and B.B. Knapf,Editors., John Wiley and Sons: Toronto, p. 287, 1974.

[33] J. B. Mohler and H. J. Sedusky, *Nickel Plating*, in *Electroplating* Chemical Publishing Co.: New York, 1951.

[34] Z. Ahmad, *Coatings*, in *Principles of Corrosion Engineering and Corrosion Control* Elsevier Ltd.: Oxford, UK, 2006.

[35] Durney, L.J.(1984*). Electroplating Engineering Handbook. 4th ed*. London: Chapman & Hall.

[36] Niece, Susan. (1990). Silver Plating On Copper, Bronze And Brass. The Antiquaries Journal. 70. 102 - 114. 10.1017/S0003581500070335.

[37] Abys, J. (2011). *Modern Electroplating, Fifth Edition*. https://doi.org/10.1002/9780470602638.ch12

[38] Liu, A., Ren, X., An, M., Zhang, J., Yang, P., Wang, B., Wang, C. (2014). A combined theoretical and experimental study for silver electroplating. Scientific reports, 4, 3837. doi:10.1038/srep03837

[39] Chandrasekar, M.S., Pushpavanam,M. (2008). Pulse and pulse reverse plating. *Central Electrochemical Research Institute*. 3313–3322

[40] O. G. Göksu, M. Erdogan, and I. Karakaya, A Pulse Voltage Application in Electrochemical Reduction of Solid CaWO4 Powder, *ECS Transactions*, 72 (33) 31-39 (2016). http://dx.doi.org/10.1149/07233.0031ecst

[41] Puippe, J. C., Leaman, F., Electroplaters, A., & Society, S. F. (1986). *Theory and Practice of Pulse Plating*. Retrieved from https://books.google.com.tr/books?id=-R-RPQAACAAJ

[42] Devaraj, G., Guruviah, S., & Seshadri, S. K. (1990). Pulse plating. *Materials Chemistry and Physics*, *25*(5), 439–461. https://doi.org/https://doi.org/10.1016/0254-0584(90)90111-M

[43] Huang, B.-C., Yang, C.-H., Lee, C.-Y., Hu, Y.-L., Hsu, C.-C., & Ho, C.-E. (2019). Effect of pulse-reverse plating on copper: Thermal mechanical properties and microstructure relationship. *Microelectronics Reliability*, *96*, 71–77. https://doi.org/https://doi.org/10.1016/j.microrel.2019.04.004

[44] Li, H., He, Y., He, T., Fan, Y., Yang, Q., & Zhan, Y. (2016). The influence of pulse plating parameters on microstructure and properties of Ni-W-Si3N4 nanocomposite coatings. *Ceramics International*, *42*(16), 18380–18392. https://doi.org/https://doi.org/10.1016/j.ceramint.2016.08.171

[45] Corresponding, C. S. (n.d.). Studies on the Effect of Base Metal Composition in Pulse Plating of Silver over Silver Alloy. 2(1), 14–18

[46] Shanthi, C., Barathan, S., Jaiswal, R., Arunachalam, R. M., & Mohan, S. (2008). *The effect of pulse parameters in electro deposition of silver alloy*. *62*, 4519–4521. https://doi.org/10.1016/j.matlet.2008.08.032

[47] Srikumar, D. S., Balasubramanian, A., Mohan, S., Raja, G., & Saravanan, G. (2008). Effect of pulse parameter on pulsed electrodeposition of copper on stainless steel. *Surface Engineering*, *25*(5), 389–392. https://doi.org/10.1179/026708408x344680

[48] Benhenda, S., jemaa, N. Ben, & Bourir, M. (1994). Effect Of Pulse Plating Parameters On Electrical Contact Behavior Of Nickel Coatings. *IEEE Transactions on Components Packaging and Manufacturing Technology Part A*, *17*(2), 303–308. https://doi.org/10.1109/95.296414

[49] Sajjadnejad, M., Omidvar, H., Javanbakht, M., & Mozafari, A. (2015). *2015(19)*. *100*(8), 1061–1065.

[50] Corporation, T. B., & Division, C. (1979). *The Bendix Corporation*.

[51] F. Ulu, G. Demirci, M. Erdoğan, İ. Karakaya, The Role of Electrolyte Composition on Codeposited Ag and Cu, ECS Transactions, 72 (21) 35-44 (2016). http://dx.doi.org/10.1149/07221.0035ecst.

[52] Durney, L.J.(1984*). Electroplating Engineering Handbook. 5th ed*. London: Chapman & Hall.

[53] Randin, J.-P. (1988). Electrochemical assessment of the tarnish resistance of decorative gold alloys. *Surface and Coatings Technology*, *34*(3), 253–275. https://doi.org/https://doi.org/10.1016/0257-8972(88)90117-X

[54] Specifications, E., Specifications, M., Certifications, C., & Data, O. (n.d.). *WR-90 Standard Gain Horn Antenna Operates From 8 . 2 GHz to 12 . 4 GHz With a Nominal 20 dB Gain SMA Female Input Connector PE9856 / SF-20 CAD Drawing*. 1–2.

[55] Baryshev, S. V., Erck, R. A., Moore, J. F., Zinovev, A. V., Tripa, C. E., & Veryovkin, I. V. (2013). Characterization of surface modifications by white light interferometry: applications in ion sputtering, laser ablation, and tribology experiments. *Journal of visualized experiments: JoVE*, (72), e50260. doi:10.3791/50260

[56] Gardiol, F. E. (1985). *Open-Ended Waveguides: Principles and Applications* (P. W. Hawkes, Ed.). In (pp. 139–187). https://doi.org/https://doi.org/10.1016/S0065-2539(08)60352-2

[57] Davies, H. (1954). The reflection of electromagnetic waves from a rough surface. *Proceedings of the IEE - Part IV: Institution Monographs*, *101*, 209–214. https://doi.org/10.1049/pi-4.1954.0025

[58] Astuti, N. H., Wibowo, N. A., & Ayub, M. R. S. S. N. (2018). The Porosity Calculation of Various Types of Paper Using Image Analysis. Jurnal Pendidikan Fisika Indonesia, 14(1), 46–51.

[59] Holzwarth, U., & Gibson, N. (2011). The Scherrer equation versus the "Debye-Scherrer equation." Nature Nanotechnology, 6, 534. https://doi.org/10.1038/nnano.2011.145

[60] Truls Norby. (2005). *Defects and transport in crystalline solids: Chapter 5: Solid state diffusion*. 1.

[61] Butrymowicz, D. B., Manning, J. R., & Read, M. E. (1975). Diffusion in copper and copper alloys. Part III. Diffusion in systems involving elements of the groups IA, IIA, IIIB, IVB, VB, VIB, and VIIB. Journal of Physical and Chemical Reference Data, 4(1), 177–250. https://doi.org/10.1063/1.555516

# APPENDICES

## A. The Results of Regression Analysis

### Regression Analysis: Roughness (μm) versus Duty Cycle

**Analysis of Variance**

| Source | DF | Adj SS | Adj MS | F-Value | P-Value |
|---|---|---|---|---|---|
| Regression | 3.00 | 0.06 | 0.02 | 77.36 | 0.00 |
| Duty Cycle (%) | 1.00 | 0.05 | 0.05 | 178.51 | 0.00 |
| Frequency (Hz) | 1.00 | 0.00 | 0.00 | 17.74 | 0.00 |
| Average Current Density (A/dm$^2$) | 1.00 | 0.01 | 0.01 | 35.82 | 0.00 |
| Error | 23.00 | 0.01 | 0.00 | | |
| Total | 26.00 | 0.07 | | | |

**Model Summary**

| S | R-sq | R-sq(adj) | R-sq(pred) |
|---|---|---|---|
| 0.0166584 | 90.98% | 89.81% | 86.96% |

**Coefficients**

| Term | Coef | SE Coef | T-Value | P-Value | VIF |
|---|---|---|---|---|---|
| Constant | 0.32 | 0.01 | 28.36 | 0.00 | |
| Duty Cycle (%) | 0.00 | 0.00 | -13.36 | 0.00 | 1.00 |
| Frequency (Hz) | 0.00 | 0.00 | 4.21 | 0.00 | 1.00 |
| Average Current Density (A/dm$^2$) | -0.05 | 0.01 | -5.99 | 0.00 | 1.00 |

**Regression Equation**

Roughness (μm) =0.32- 0.001 Duty Cycle (%) + 0.0005 Frequency (Hz) -

0.05 Average Current Density (A/dm$^2$)

**Fits and Diagnostics for Unusual Observations**

| Roughness (μm) | Fit | Resid | Std Resid |
|---|---|---|---|
| 0.24 | 0.20 | 0.04 | 2.32 |

## B. % Dark Region Calculation from SEM Images
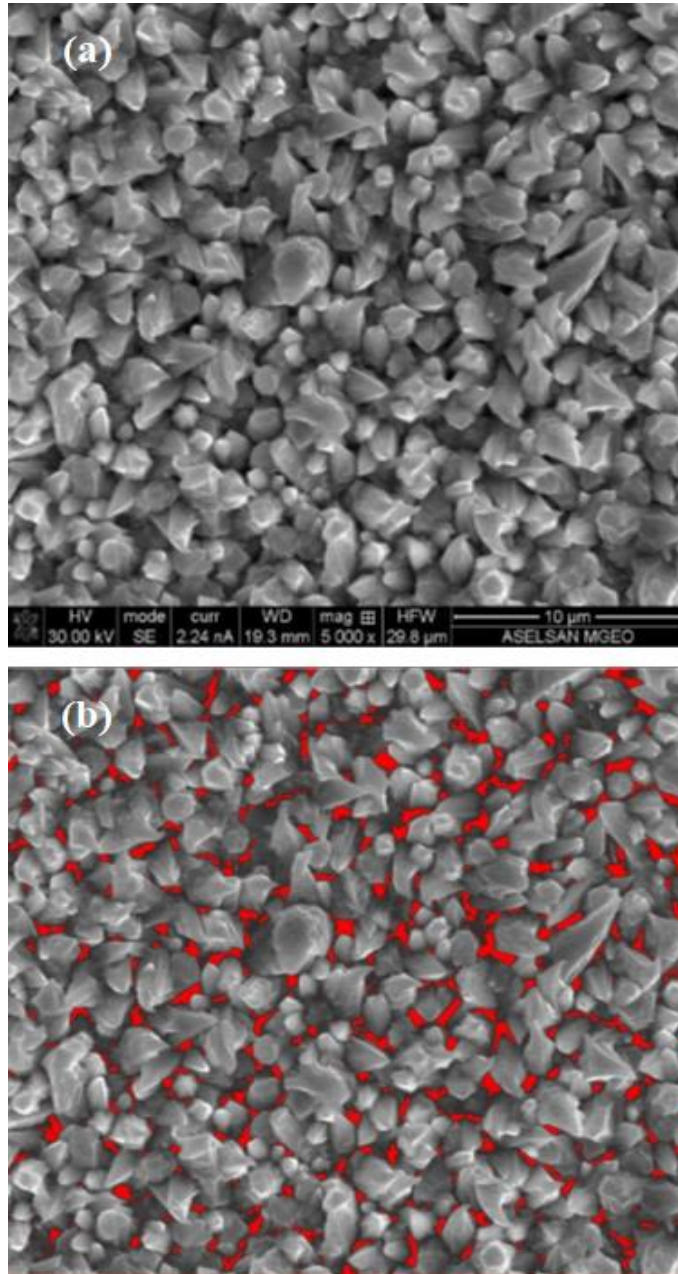


(a) SEM image of a pulse silver plating at 75 Duty Cycle (%) 80 Frequency (Hz) 1.5 Average
Current Density (A/dm$^2$) (b) black area pointed out in red after image thresholding

% Dark Region: 3.9
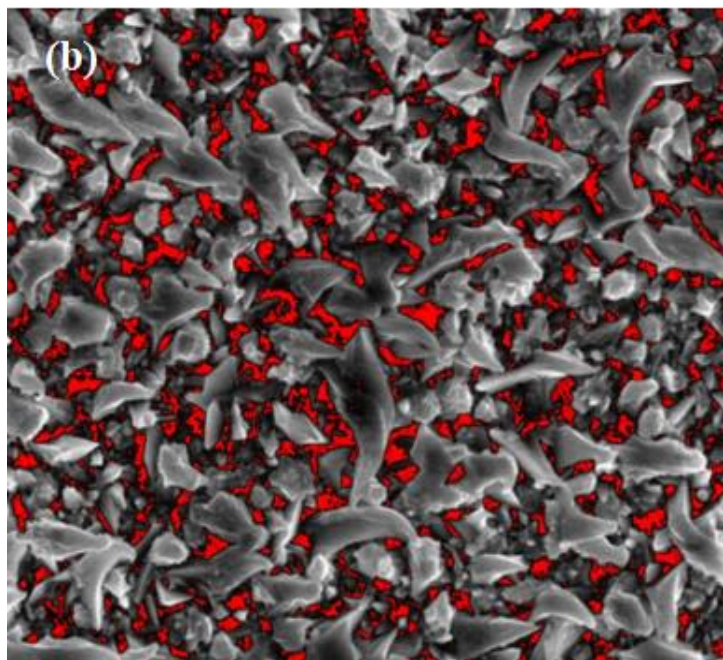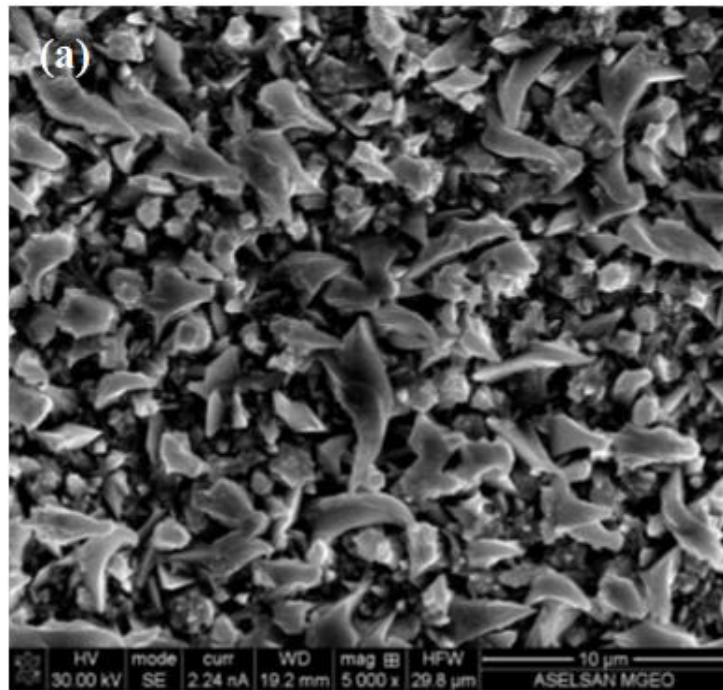
**(a) SEM image of a pulse silver plating at 75 Duty Cycle (%) 80 Frequency (Hz) 0.5 Average Current Density (A/dm²) (b) black area pointed out in red after image thresholding**

**% Dark Region: 4.4**
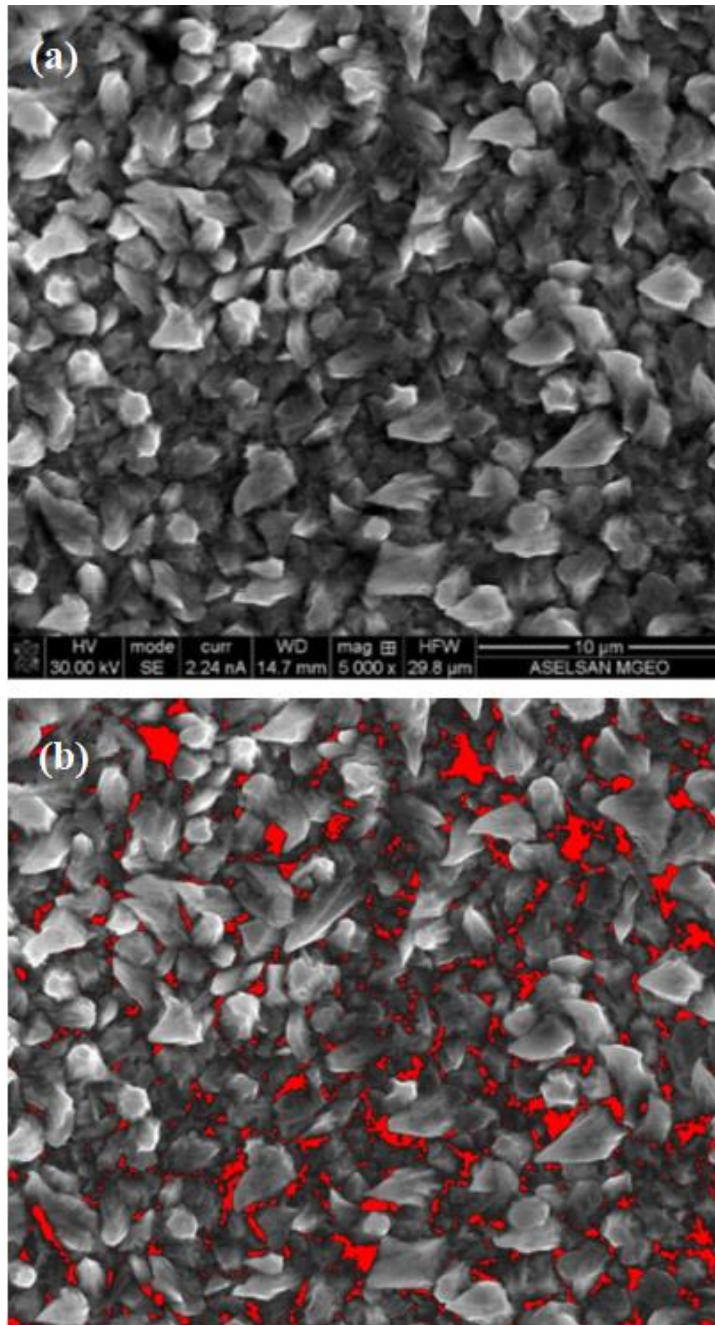
**(a) SEM image of a pulse silver plating at 75 Duty Cycle (%) 10 Frequency (Hz) 1.5 Average Current Density (A/dm$^2$) (b) black area pointed out in red after image thresholding**

**% Dark Region: 5.8**
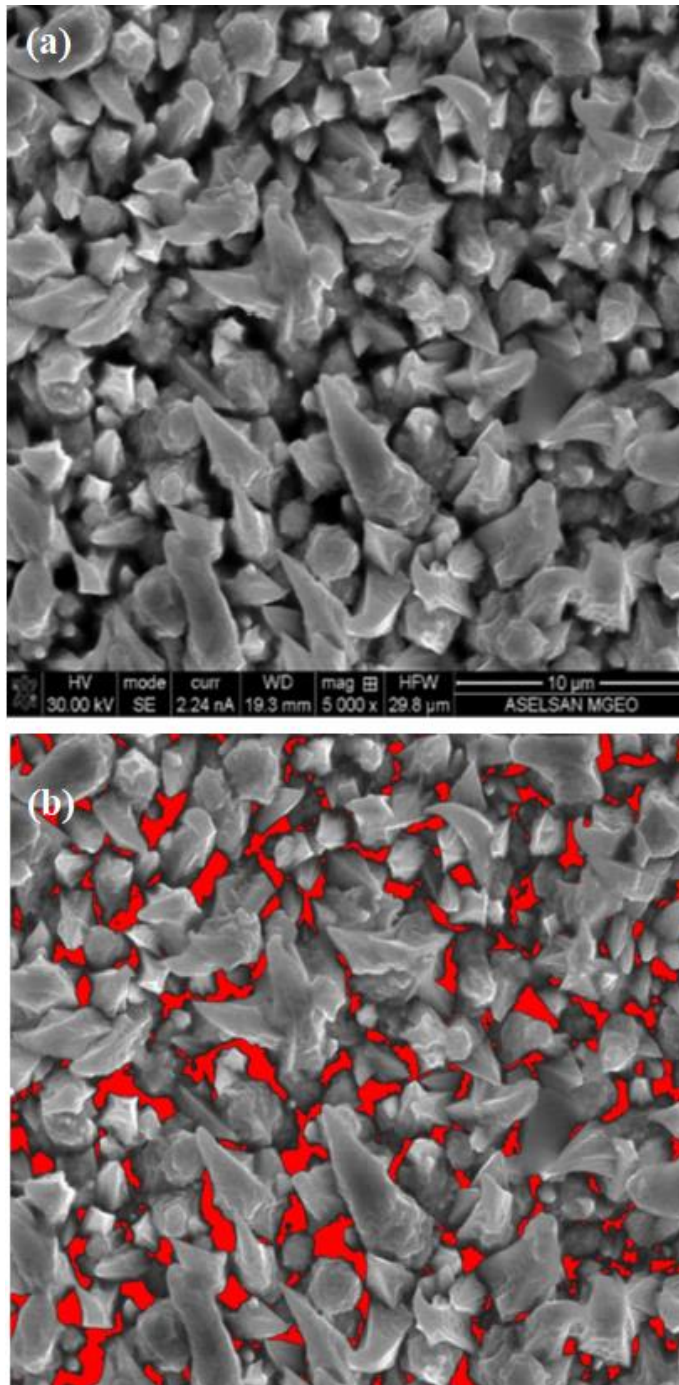
**(a) SEM image of a pulse silver plating at 75 Duty Cycle (%) 10 Frequency (Hz) 0.5 Average Current Density (A/dm$^2$) (b) black area pointed out in red after image thresholding**

**% Dark Region: 6.2**
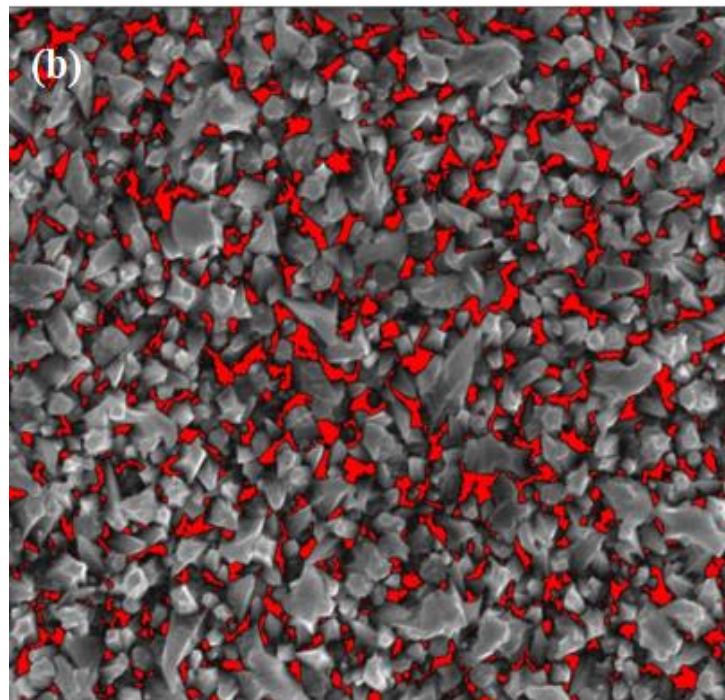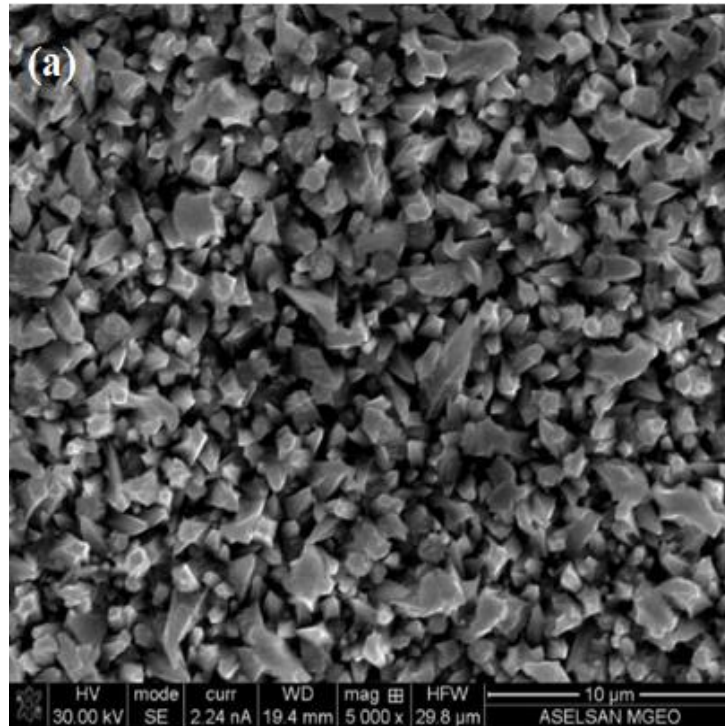
**(a) SEM image of a pulse silver plating at 75 Duty Cycle (%) 40 Frequency (Hz) 0.5 Average Current Density (A/dm$^2$) (b) black area pointed out in red after image thresholding**

**% Dark Region: 6.3**
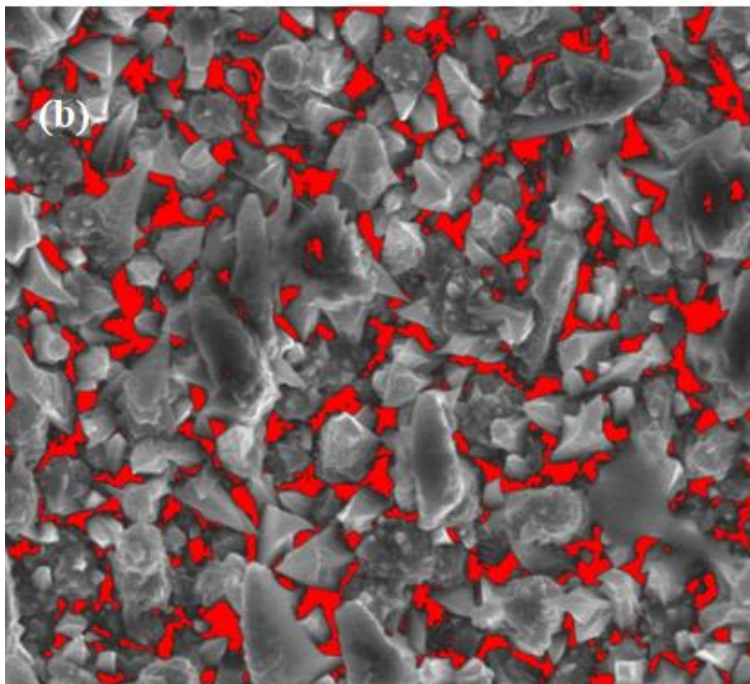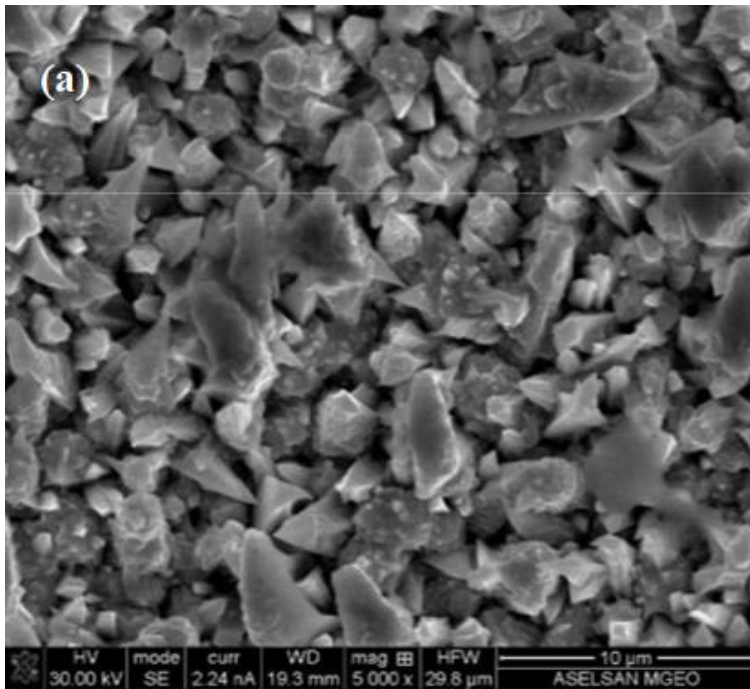
**(a) SEM image of a pulse silver plating at 10 Duty Cycle (%) 10 Frequency (Hz) 1 Average Current Density (A/dm$^2$) (b) black area pointed out in red after image thresholding**

**% Dark Region: 9.5**

## C. Silver Crystallite Size Calculation

**Grain size and plating condition of coupon 27**

| Ag crystallite size (nm) | Duty Cycle (%) | Frequency (Hz) | Average Current Density (A/dm$^2$) |
|---|---|---|---|
| 48.7 | 75 | 10 | 1,5 |

**Full width at half maximum (FWHM) calculation of coupon 27**

| Peak position 2θ (°) | FWHM B$_{size}$ (°) | Dp (nm) |
|---|---|---|
| 38.17 | 0.13163 | 66.75 |
| 44.34 | 0.21108 | 42.48 |
| 64.51 | 0.18011 | 54.52 |
| 77.47 | 0.34293 | 31.04 |
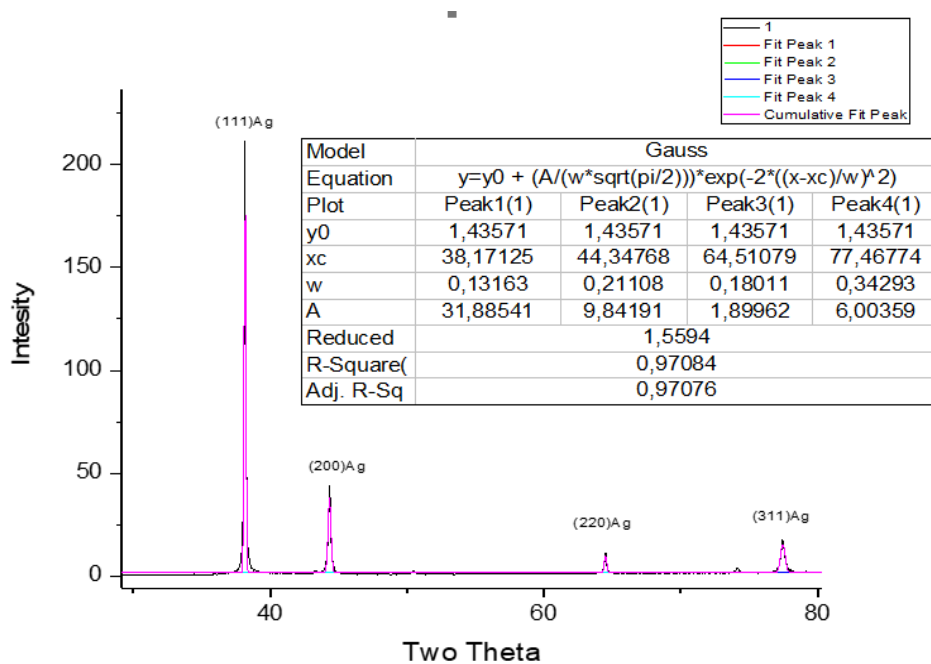


**X-Ray diffraction (XRD) patterns of coupon 27**

# Calculation of FHWM and Grain Size of Coupon 24

**Grain size and plating condition of coupon 24**

| Ag crystallite size (nm) | Duty Cycle (%) | Frequency (Hz) | Average Current Density (A/dm²) |
|---|---|---|---|
| 42.13 | 75 | 80 | 1 |

**Full width at half maximum (FWHM) calculation of coupon 24**

| Peak position 2θ (°) | FWHM B$_{size}$ (°) | Dp (nm) |
|---|---|---|
| 38.16 | 0.1336 | 65.77 |
| 44.35 | 0.24766 | 36.21 |
| 64.51 | 0.24268 | 40.46 |
| 77.47 | 0.40811 | 26.08 |
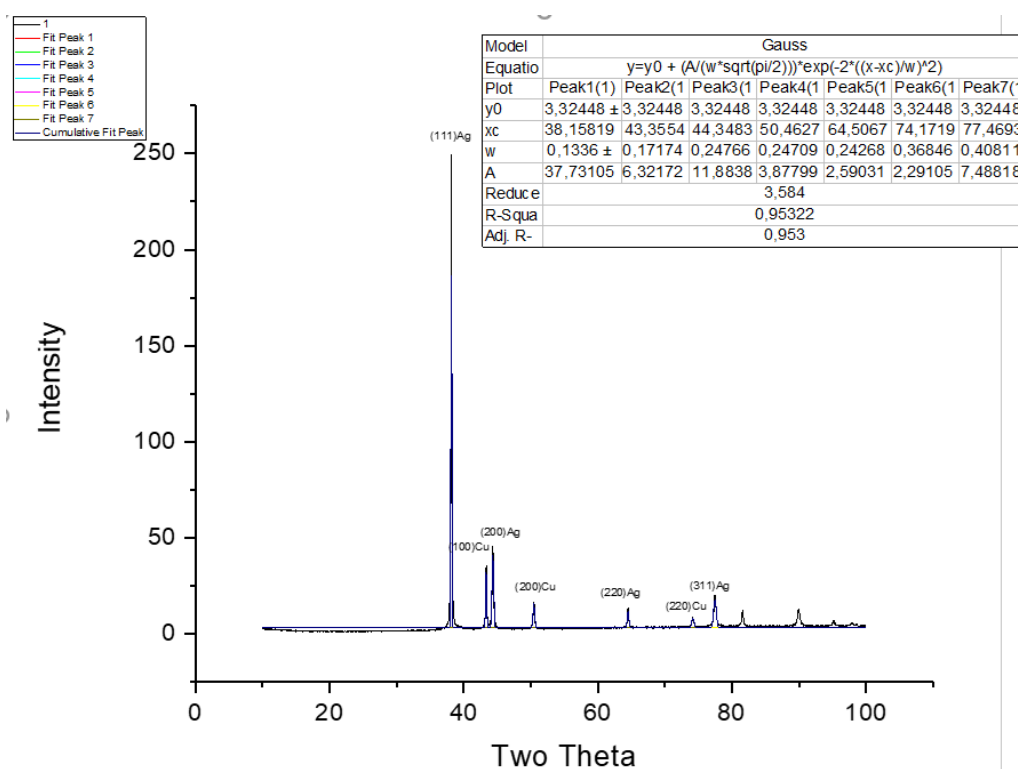


**X-Ray diffraction (XRD) patterns of coupon 24**

# Calculation of FHWM and Grain Size of Coupon 18

**Grain size and plating condition of coupon 18**

| Ag crystallite size (nm) | Duty Cycle (%) | Frequency (Hz) | Average Current Density (A/dm$^2$) |
|---|---|---|---|
| 48,64 | 75 | 80 | 0,5 |

**Full width at half maximum (FWHM) calculation of coupon 18**

| Peak position 2θ (°) | FWHM B$_{size}$ (°) | Dp (nm) |
|---|---|---|
| 38.13 | 0.12837 | 68.44 |
| 44.31 | 0.22539 | 39.78 |
| 64.48 | 0.18475 | 53.14 |
| 77.43 | 0.32034 | 33.22 |



| Model | Gauss | | | | | | |
|---|---|---|---|---|---|---|---|
| Equatio | y=y0 + (A/(w*sqrt(pi/2)))*exp(-2*((x-xc)/w)^2) | | | | | | |
| Plot | Peak1(2) | Peak2(2) | Peak3(2 | Peak4(2 | Peak5(2 | Peak6(2 | Peak7(2 |
| y0 | 5,76808 ± | 5,76808 ± | 5,76808 | 5,76808 | 5,76808 | 5,76808 | 5,76808 |
| xc | 38,13407 | 43,31817 | 44,3161 | 50,4184 | 64,4830 | 74,1369 | 77,4374 |
| w | 0,12837 ± | 0,16078 ± | 0,22539 | 0,25064 | 0,18475 | 0,30272 | 0,32074 |
| A | 14,40097 | 22,69611 | 5,42978 | 13,2626 | 2,11343 | 6,1303 ± | 2,57386 |
| Reduce | 3,10915 | | | | | | |
| R-Squa | 0,92073 | | | | | | |
| Adj. R- | 0,92035 | | | | | | |
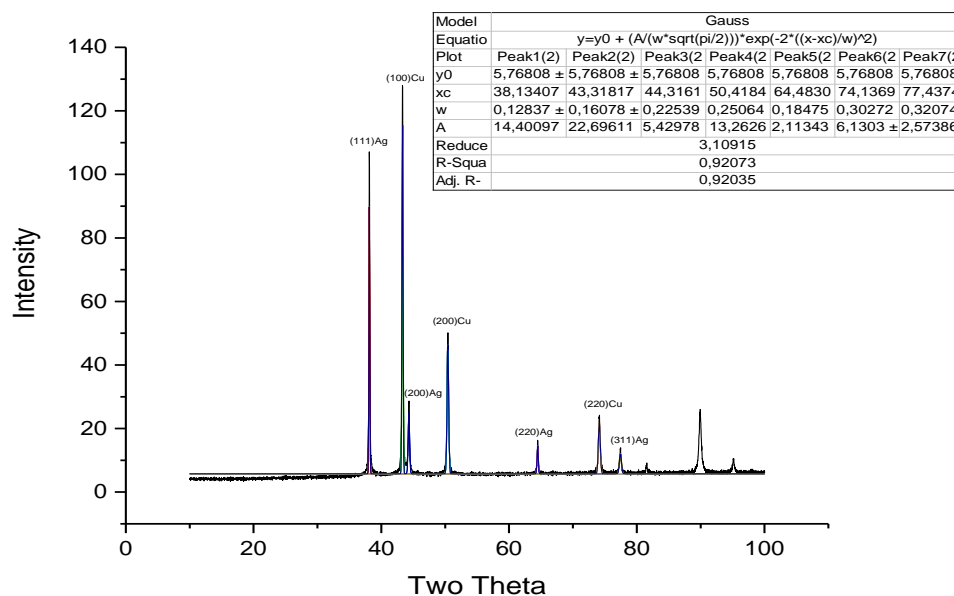
**X-Ray diffraction (XRD) patterns of coupon 18**

## Calculation of FHWM and Grain Size of Coupon 26

**Grain size and plating condition of coupon 26**

| Ag crystallite size (nm) | Duty Cycle (%) | Frequency (Hz) | Average Current Density (A/dm$^2$) |
|---|---|---|---|
| 40,92 | 75 | 80 | 1,5 |

**Full width at half maximum (FWHM) calculation of coupon 26**

| Peak position 2θ (°) | FWHM B$_{size}$ (°) | Dp (nm) |
|---|---|---|
| 38.1 | 0.141259 | 62.19 |
| 44.28 | 0.23839 | 37.61 |
| 64.44 | 0.26337 | 37.27 |
| 77.41 | 0.4 | 26.60 |
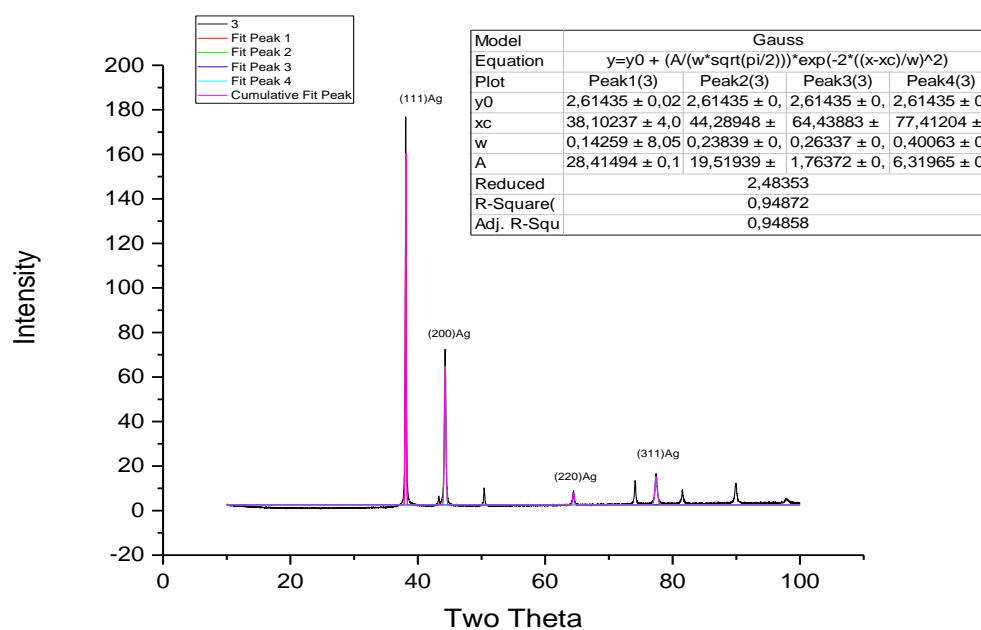


**X-Ray diffraction (XRD) patterns of coupon 26**

# Calculation of FHWM and Grain Size of Coupon 7

**Grain size and plating condition of coupon 7**

| Ag crystallite size (nm) | Duty Cycle (%) | Frequency (Hz) | Average Current Density (A/dm$^2$) |
|---|---|---|---|
| 70,74 | 10 | 10 | 1 |

**Full width at half maximum (FWHM) calculation of coupon 7**

| Peak position 2θ (°) | FWHM B$_{size}$ (°) | Dp (nm) |
|---|---|---|
| 38.18 | 0.08846 | 99.33 |
| 44.36 | 0.15343 | 58.45 |
| 64.5 | 0.13722 | 71.55 |
| 77.46 | 0.19848 | 53.63 |



| Model | Gauss | | | |
|---|---|---|---|---|
| Equation | y=y0 + (A/(w*sqrt(pi/2)))*exp(-2*((x-xc)/w)^2) | | | |
| Plot | Peak1(1) | Peak2(1) | Peak3(1) | Peak4(1) |
| y0 | 2,17798 ± 0,02 | 2,17798 ± 0,0 | 2,17798 ± 0,0 | 2,17798 ± 0,0 |
| xc | 38,18074 ± 3,6 | 44,36097 ± 0, | 64,50885 ± 0, | 77,45786 ± 0, |
| w | 0,08846 ± 7,37 | 0,15343 ± 0,0 | 0,13722 ± 0,0 | 0,19848 ± 0,0 |
| A | 14,04165 ± 0,1 | 3,56821 ± 0,1 | 3,30599 ± 0,1 | 3,30843 ± 0,1 |
| Reduced C | 2,12921 | | | |
| R-Square(C | 0,87787 | | | |
| Adj. R-Squa | 0,87754 | | | |
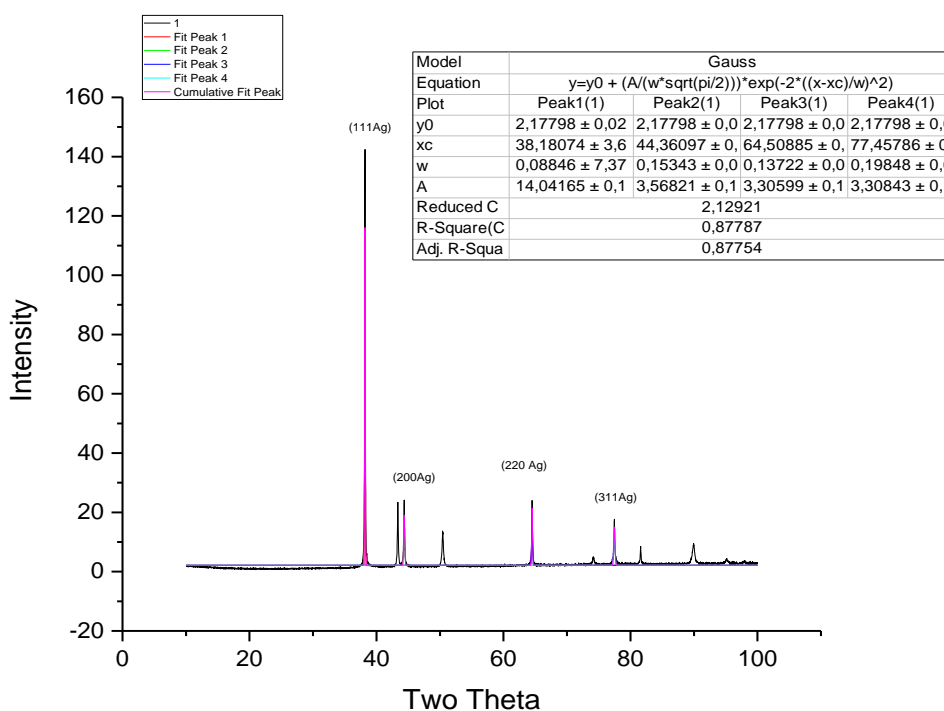
**X-Ray diffraction (XRD) patterns of coupon 7**

# Calculation of FHWM and Grain Size of Coupon 16

**Grain size and plating condition of coupon 16**

| Ag crystallite size (nm) | Duty Cycle (%) | Frequency (Hz) | Average Current Density (A/dm$^2$) |
|---|---|---|---|
| 63,09 | 50 | 10 | 1 |

**Full width at half maximum (FWHM) calculation of coupon 16**

| Peak position 2θ (°) | FWHM B$_{size}$ (°) | Dp (nm) |
|---|---|---|
| 38.16 | 0.094 | 93.47 |
| 44.34 | 0.16983 | 52.80 |
| 64.49 | 0.1574 | 62.38 |
| 77.44 | 0.24345 | 43.72 |
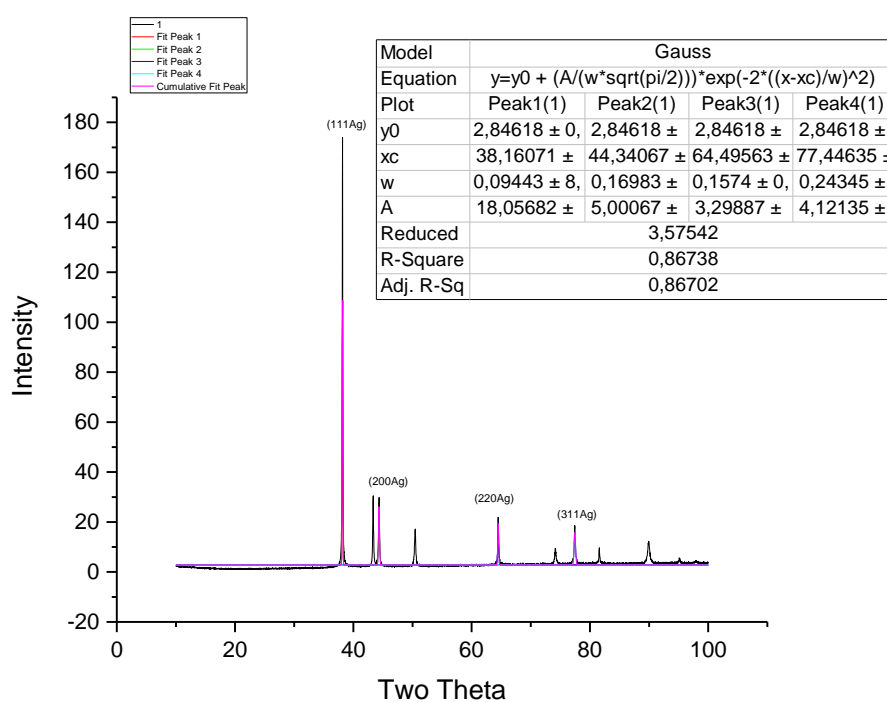


**X-Ray diffraction (XRD) patterns of coupon 16**

# Calculation of FHWM and Grain Size of Coupon 14

**Grain size and plating condition of coupon 14**

| Ag crystallite size (nm) | Duty Cycle (%) | Frequency (Hz) | Average Current Density (A/dm$^2$) |
|---|---|---|---|
| 59,09 | 75 | 40 | 0,5 |

**Full width at half maximum (FWHM) calculation of coupon 14**

| Peak position 2θ (°) | FWHM B$_{size}$ (°) | Dp (nm) |
|---|---|---|
| 38.17 | 0.10849 | 80.99 |
| 44.35 | 0.177 | 50.66 |
| 64.5 | 0.13764 | 71.33 |
| 77.46 | 0.319 | 33.37 |

| Model | Gauss | | | |
|---|---|---|---|---|
| Equation | y=y0 + (A/(w*sqrt(pi/2)))*exp(-2*((x-xc)/w)^2) | | | |
| Plot | Peak1(2) | Peak2(2) | Peak3(2) | Peak4(2) |
| y0 | 2,86907 ± 0, | 2,86907 ± | 2,86907 ± | 2,86907 ± |
| xc | 38,17181 ± | 44,35633 ± | 64,50301 ± | 77,46142 ± |
| w | 0,10849 ± 8, | 0,17779 ± | 0,13764 ± | 0,319 ± 0,0 |
| A | 19,66239 ± | 5,15555 ± | 2,16998 ± | 4,12385 ± |
| Reduced | 3,24643 | | | |
| R-Square | 0,87982 | | | |
| Adj. R-Sq | 0,87949 | | | |
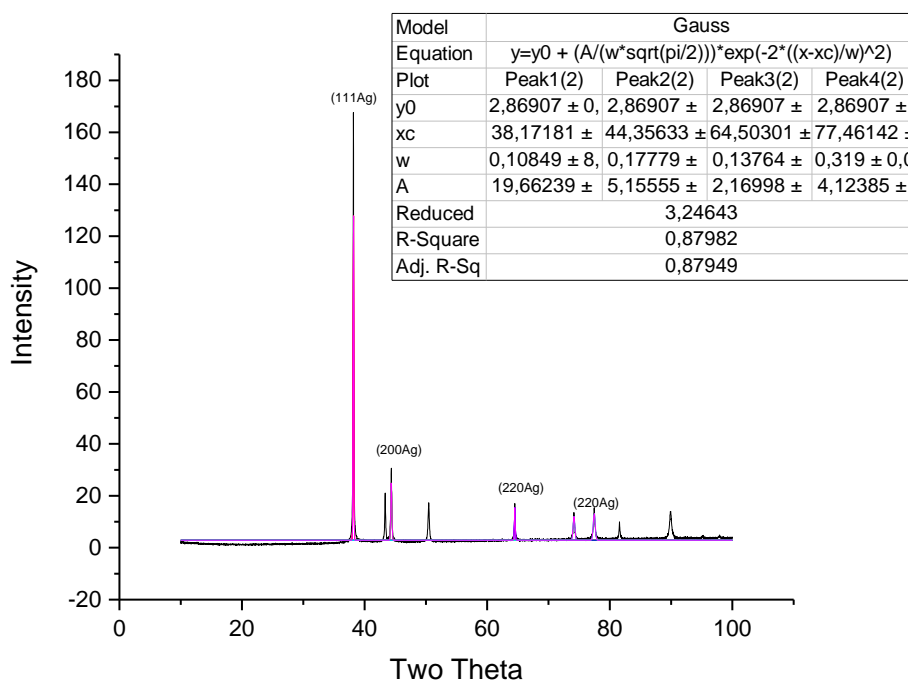
**X-Ray diffraction (XRD) patterns of coupon 14**

## Calculation of FHWM and Grain Size of Coupon 20

**Grain size and plating condition of coupon 20**

| Ag crystallite size (nm) | Duty Cycle (%) | Frequency (Hz) | Average Current Density (A/dm$^2$) |
|---|---|---|---|
| 59,12 | 75 | 10 | 0,5 |

**Full width at half maximum (FWHM) calculation of coupon 20**

| Peak position 2θ (°) | FWHM B$_{size}$ (°) | Dp (nm) |
|---|---|---|
| 38.1723 | 0.11485 | 76.51 |
| 43.36 | 0.1504 | 59.41 |
| 64.5 | 0.166 | 59.15 |
| 77.45 | 0.25696 | 41.42 |



| Model | Gauss | | | |
|---|---|---|---|---|
| Equation | y=y0 + (A/(w*sqrt(pi/2)))*exp(-2*((x-xc)/w)^2) | | | |
| Plot | Peak1(2) | Peak2(2) | Peak3(2) | Peak4(2) |
| y0 | 4,25963 ± 0, | 4,25963 ± | 4,25963 ± | 4,25963 ± |
| xc | 38,17233 ± 9 | 43,36003 ± | 64,50898 ± | 77,45554 ± |
| w | 0,11485 ± 0, | 0,1504 ± 0 | 0,16671 ± | 0,25696 ± |
| A | 13,36754 ± 0 | 17,95698 ± | 2,02004 ± | 2,32694 ± |
| Reduced | 6,3984 | | | |
| R-Square | 0,78515 | | | |
| Adj. R-Sq | 0,78456 | | | |
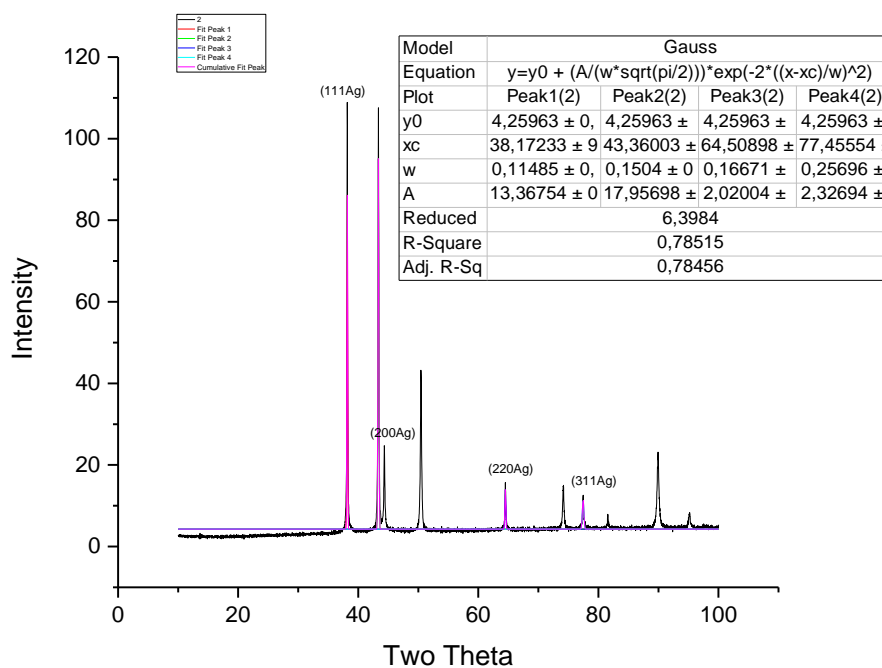
**X-Ray diffraction (XRD) patterns of coupon 20**

## D. SEM Images and Ag Contents versus Distance Graphs of EDS Analysis
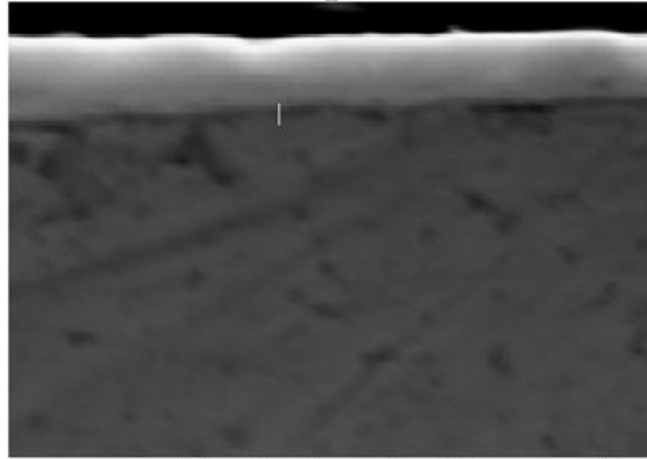


**SEM image for No 26**
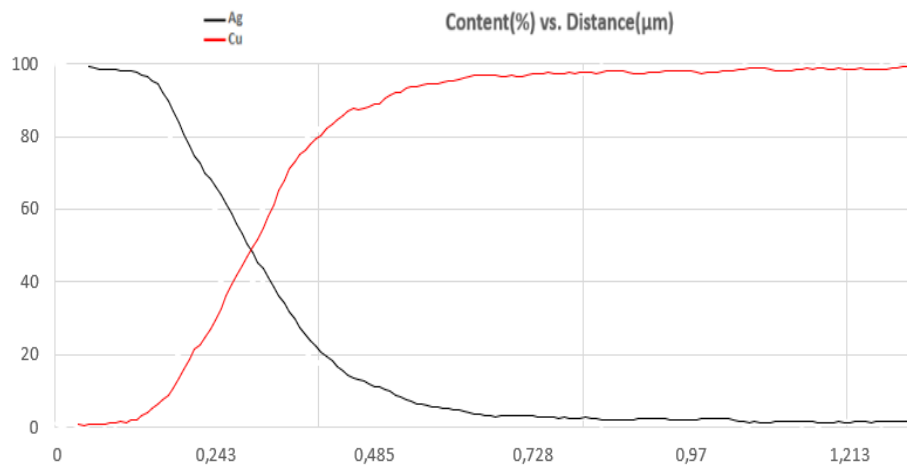


**Ag contents versus distance graph for No 26**
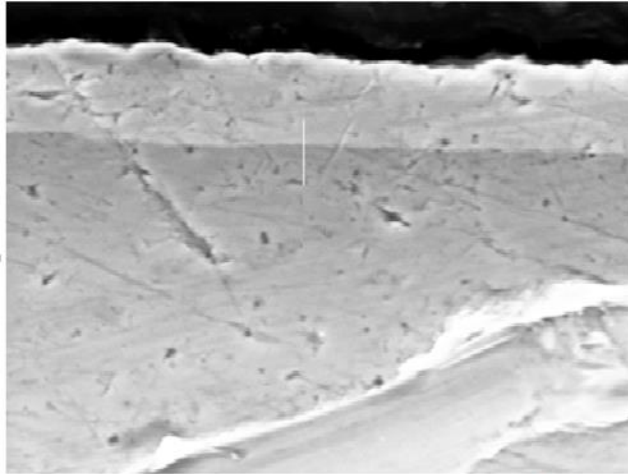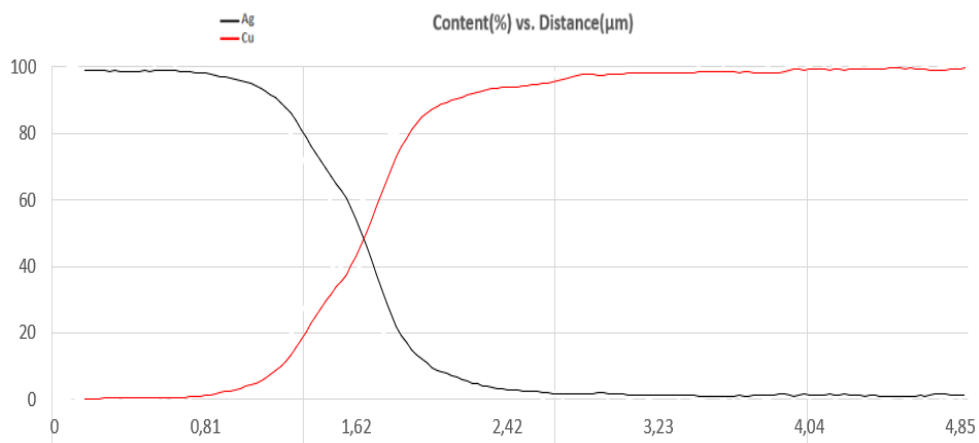
**SEM image for No 14**



**Ag contents versus distance graph for No 14**
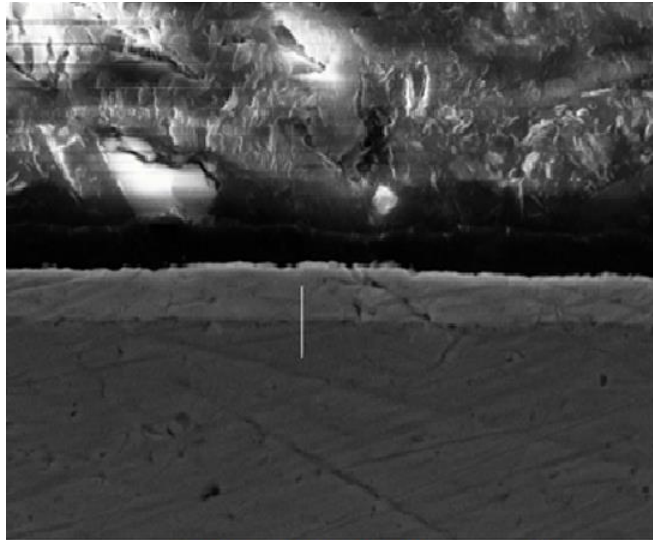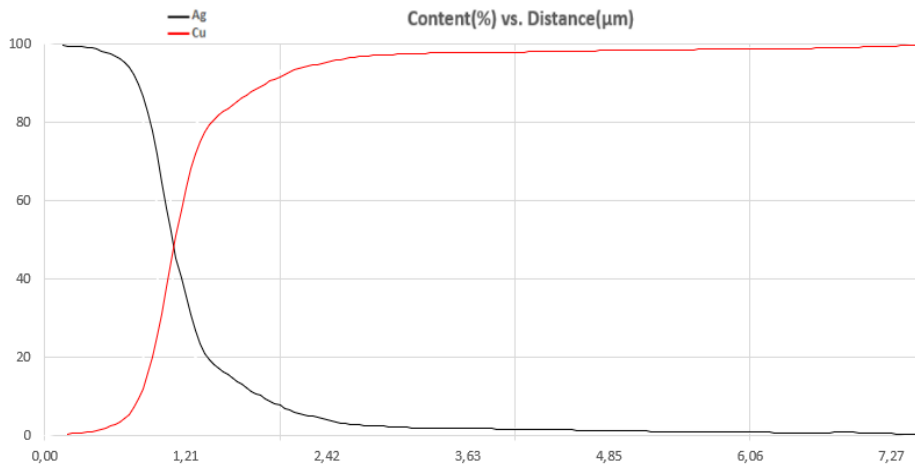
**SEM image for No 16**



**Ag contents versus distance graph for No 16**
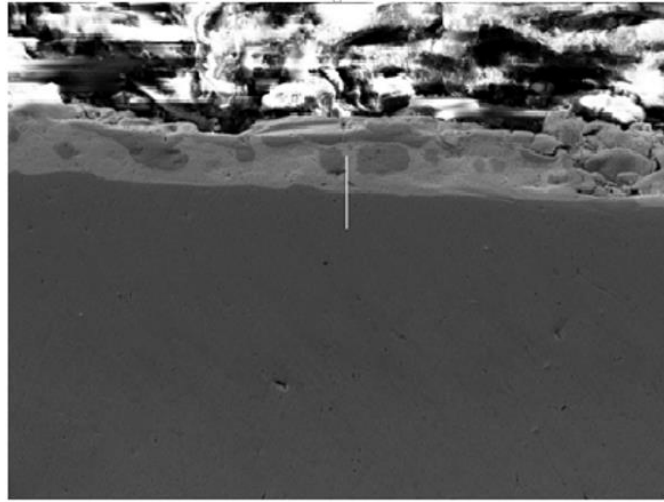
**SEM image for No 7**



**Ag contents versus distance graph for No 7**